



# 1 A new global dataset of mountain glacier centerline and length

2 Dahong Zhang<sup>1,2</sup>, Gang Zhou<sup>1,2</sup>, Wen Li<sup>1,2</sup>, Shiqiang Zhang<sup>1,2</sup>, Xiaojun Yao<sup>3</sup>, Shimei Wei<sup>3</sup>

3 <sup>1</sup> College of Urban and Environmental Science, Northwest University, Xi'an 710127, PR China

4 <sup>2</sup> Shaanxi Key Laboratory of Earth Surface System and Environmental Carrying Capacity, Northwest University,  
5 Xi'an 710127, PR China

6 <sup>3</sup> College of Geography and Environment Sciences, Northwest Normal University, Lanzhou 730070, PR China

7 Correspondence: Shiqiang Zhang (zhangsq@lzb.ac.cn)

8  
9 **Abstract.** Length is one of the key determinants of glacier geometry and is an important parameter  
10 of glacier inventory and modeling; glacier centerlines are crucial inputs for many glaciological  
11 applications. In this study, the centerlines and maximum lengths of global glaciers were extracted  
12 using an automatic extraction algorithm based on the latest global glacier inventory data, digital  
13 elevation data (DEM), and European allocation theory. The glacier polygons were reconstructed  
14 according to the geometric principle and an automatic checking algorithm for the global glacier  
15 outlines was designed to filter erroneous or unsupported glacier outlines. The DEMs of global  
16 glacier-covered regions were compiled using available DEMs. An updated automatic extraction tool  
17 was designed independently, and a parameterization scheme with empirical thresholds was applied  
18 for data production. The accuracy of the dataset was evaluated using random assessment with visible  
19 interpretation and comparative analysis with another dataset. The 10,764 erroneous glacier polygons,  
20 7,174 ice caps, and 419 nominal glaciers from the Randolph Glacier Inventory (RGI) version 6.0  
21 were identified and excluded, accounting for 8.25% of the total. In total, 198,137 glacier centerlines  
22 were generated, accounting for 99.74% of the total input glaciers and 91.52% of the RGI v6.0. The  
23 accuracy of glacier centerlines was 89.68%. The comparison between the dataset and previous  
24 datasets suggested that the majority of glacier centerlines were slightly longer than those in RGI  
25 v6.0. The extraction method of this study has a strong ability to obtain the maximum length of  
26 glaciers, meaning that the maximum lengths of some glaciers were likely underestimated in the past.  
27 The dataset constructed includes 14 sub-datasets, such as the global glacier centerline dataset, global  
28 glacier maximum length dataset, and global glacier DEM dataset, all of which can be found at link:  
29 <https://doi.org/10.11922/sciencedb.01643> (Zhang and Zhang, 2022).

## 31 1 Introduction

32 Mountain glaciers which are distinct from the Greenland and Antarctic ice sheets, are also shrinking  
33 rapidly (Hugonnet et al., 2021). They are altering regional hydrology (Pritchard, 2019), raising  
34 global sea levels (Cazenave, 2018), and elevating natural hazards (Shukla and Sen, 2021; Zheng et  
35 al., 2021). These glaciers are among the most climate-sensitive constituents of the world's natural  
36 water towers (Immerzeel et al., 2019). Under the influence of global climate change, studies on  
37 glacier area changes (Sommer et al., 2020; Li et al., 2021), ice thickness (Farinotti et al., 2019), mass  
38 balance (Zemp et al., 2019; Vargo et al., 2020; Wu et al., 2021), ice velocity field (Thogersen et al.,  
39 2019), the impact of debris-cover (Scherler et al., 2018; Shukla et al., 2020; Herreid and Pellicciotti,  
40 2020), glacier meltwater (Noel et al., 2020), sediment release (Aciego et al., 2015; Li et al., 2019),  
41 and related hazards (Zhou et al., 2021b; Stuart-Smith et al., 2021; Käab et al., 2021) in glacier-  
42 covered regions are essential for global water resources supply and disaster prevention and reduction.

43



44 The most obvious distinction between glaciers and other natural ice bodies is their property to move  
45 towards lower altitudes under the influence of gravity. Glacier flow lines are the motion trajectories  
46 of a glacier and the main flow line is the key trajectory. The main flow line cannot be obtained on a  
47 large scale owing to the lack of glacier velocity field data. The glacier centerline, generated via the  
48 axis line method (Le Bris and Paul, 2013; Machguth and Huss, 2014; Kienholz et al., 2014; Zhang  
49 et al., 2021), is typically used to represent the main flow line. The glacier centerline is a critical  
50 parameter for analyzing the ice velocity field (Heid and Käab, 2012; Melkonian et al., 2017),  
51 estimating the glacier volume (Li et al., 2012; Gao et al., 2018), and developing glacier models  
52 (Oerlemans, 1997; Sugiyama et al., 2007; Maussion et al., 2019).

53  
54 Glacier length, usually referring to the maximum length of a glacier centerline (main flow line),  
55 represents the longest motion trajectory of a glacier, which is one of the key determinants of glacier  
56 geometry and a basic parameter of glacier inventories (RGI Consortium, 2017) and modeling  
57 (Maussion et al., 2019). Glacier length fluctuations can be used to quantify glacier changes (Zhou  
58 et al., 2021a), such as by identifying glacier advancement, surge, or retreat. Glacier length  
59 fluctuations (e.g., Leclercq et al., 2014) have also been used to study the relationships with changes  
60 in glacier area (Winsvold et al., 2014) and the geometric structure of a glacier (Herla et al., 2017),  
61 estimate glacier volume in combination with the glacier area (Lüthi et al., 2010), and reconstruct  
62 annual averaged surface temperatures over the past 400 years on hemispherical and global scales  
63 (Leclercq and Oerlemans, 2011).

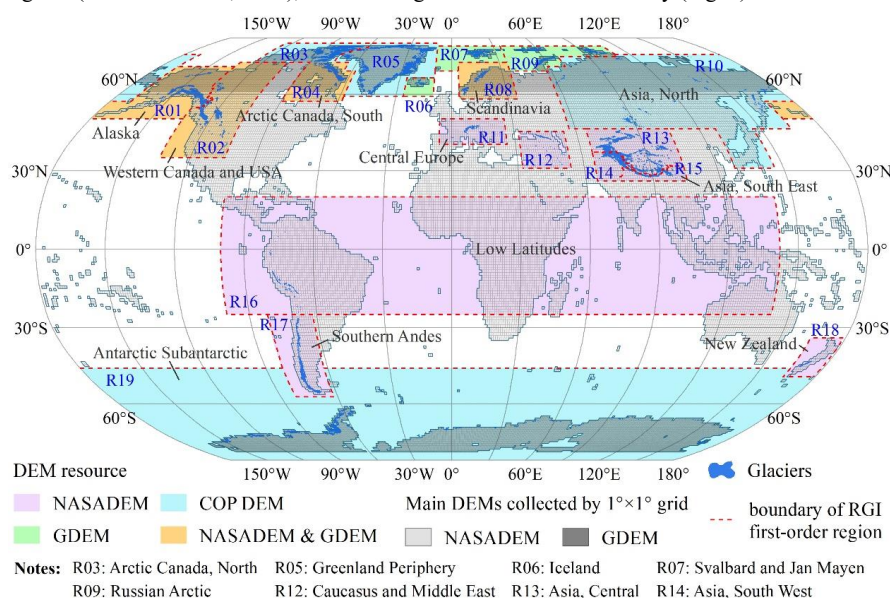
64  
65 The global complete inventory (RGI Consortium, 2017) of glacier outlines was created following  
66 the Fifth Assessment Report of the Intergovernmental Panel on Climate Change (IPCC AR5). To  
67 meet the demand for large-scale acquisition of glacier length, automatic and semi-automatic  
68 methods have been proposed. There are three types of methods: first, the typical hydrological  
69 analysis method (Schiefer et al., 2008), but the lengths are longer than equivalent maximum  
70 distances taken along typical longitudinal centerline profiles; second, a simplified algorithm based  
71 on skeleton theory (Le Moine and Gsell, 2015), but this method has not been widely used; third,  
72 centerline method based on the axis concept, proposed by Le Bris and Paul (2013), and applied to  
73 the calculation of global glacier length for the first time by Machguth and Huss (2014). However, it  
74 is difficult to extract complex glaciers using the method of (Le Bris and Paul, 2013). The cost grid-  
75 least-cost route approach of Kienholz et al. (2014) based on the axis concept has higher accuracy,  
76 but it requires more labor and time, which limits its application to global glaciers. The trade-off  
77 function approach of Machguth and Huss (2014) was based on the axis concept; the results cover  
78 almost all mountain glaciers in the world but exclude the centerlines of branches of glaciers.  
79 Therefore, researchers have been trying to overcome these difficulties in recent years (Yao et al.,  
80 2015; Yang et al., 2016; Ji et al., 2017; Hansen et al., 2020; Xia, 2020; Zhang et al., 2021). To date,  
81 global datasets of the centerline and length of mountain glaciers are rare, including that of glacier  
82 branches. Based on our recent study (Zhang et al., 2021) on successfully extracting the glacier  
83 centerline using the Euclidean allocation, in this study, we aim to combine free, available digital  
84 elevation data into one global digital elevation model (DEM) with 30 m resolution from 90°N to  
85 90°S, check and correct the global glacier outlines, and obtain a new graphic dataset of the centerline  
86 and length for global mountain glaciers based on the updated DEM and outlines.

87



88 **2 Study region and data**

89 The glacier dataset used in this study was the RGI version 6.0  
 90 (<http://www.glims.org/RGI/randolph.html>, last accessed: 15 November 2021) released via the  
 91 Global Land Ice Measurements from Space initiative (GLIMS), which is a globally complete  
 92 collection of digital outlines of glaciers, excluding ice sheets (Pfeffer et al., 2014). RGI v6.0 includes  
 93 216,502 glaciers (215,547 glaciers described in the product handbook) worldwide, with a total area  
 94 of 705,738.793 km<sup>2</sup> (RGI Consortium, 2017). All glaciers can be divided into 19 first-order glacier  
 95 regions (Radić and Hock, 2010), and these regions were used in our study (Fig. 1).



96 **Figure 1.** Distribution of global glaciers, first-order glacier regions, and DEMs. The background is  
 98 the global DEM grid (1°×1°) covered by NASADEM and GDEM. GDEM and COP DEM represent  
 99 the ASTER GDEM v3 and the Copernicus DEM, respectively.

100  
 101 Five DEM products (Table 1) were collected in preliminary studies. The National Aeronautics and  
 102 Space Administration (NASA) DEM (NASADEM) ([https://lpdaac.usgs.gov/news/release-](https://lpdaac.usgs.gov/news/release-nasadem-data-products/)  
 103 [nasadem-data-products/](https://lpdaac.usgs.gov/news/release-nasadem-data-products/), last accessed: November 17, 2021) was released by the Land Processes  
 104 Distributed Active Archive Center (LP DAAC) in January 2020. As a modernization of the DEM  
 105 and associated products generated from the Shuttle Radar Topography Mission (SRTM) data (Farr  
 106 et al., 2007), the NASADEM, with a low mean absolute error (MAE) (Carrera-Hernández, 2021),  
 107 is the successor of the NASA SRTM V3. The root mean square error (RMSE) of NASADEM is  
 108 better than that of SRTM (Uuemaa et al., 2020). Serving the zonal extent of (56°S, 61°N),  
 109 NASADEM was used as the preferred DEM in this study because of its superior performance. The  
 110 Advanced Spaceborne Thermal Emission and Reflection Radiometer (ASTER) is a 14-channel  
 111 imaging instrument operating on the Terra satellite of NASA since 1999. ASTER Global Digital  
 112 Elevation Model (GDEM) version 3 ([https://lpdaac.usgs.gov/news/nasa-and-meti-release-aster-](https://lpdaac.usgs.gov/news/nasa-and-meti-release-aster-global-dem-version-3/)  
 113 [global-dem-version-3/](https://lpdaac.usgs.gov/news/nasa-and-meti-release-aster-global-dem-version-3/), last accessed: November 17, 2021) (Abrams et al., 2020) was released by  
 114 Japan’s Ministry of Economy, Trade, and Industry (METI) and NASA in July 2019. Using ICESat



115 data, Carabajal and Boy (2016) found that ASTER GDEM v3 displayed smaller means, similar  
116 medians, and less scatter than ASTER GDEM v2 in Greenland and Antarctica. To determine the  
117 zonal extent of (56°S, 83°S) and (61°N, 83°N), ASTER GDEM v3 was used as the second priority  
118 DEM in this study.

119  
120 NASADEM and ASTERGDEM v3 do not cover all glacierized regions, missing parts of the polar  
121 region and the Kamchatka Peninsula. Because of their high temporal and spatial resolution at high  
122 latitudes, the reference elevation model of Antarctica (REMA) (Howat et al., 2019) and ArcticDEM  
123 (<https://www.pgc.umn.edu/data/arcticdem/>, last accessed: November 17, 2021) were preferred as  
124 the supplementary data of our preliminary studies in these glacier regions. However, ArcticDEM  
125 and REMA are not suitable because of insufficient coverage and sporadic data. Therefore,  
126 Copernicus DEM (<https://spacedata.copernicus.eu/web/cscda/cop-dem-faq>, last accessed:  
127 November 17, 2021) with a wide coverage was finally determined as the supplementary data for  
128 glacier regions not covered via the NASADEM and ASTER GDEM v3 completely. The Copernicus  
129 DEM was recently released (November 2020) and the accuracy assessment undertaken by its  
130 development team (the product handbook) using TanDEM-X DEM/World DEM ICESat GLAS  
131 reference points found an absolute vertical accuracy of approximately 10 m at the periphery of  
132 Antarctica and Greenland. Finally, NASADEM, ASTER GDEM v3, and Copernicus DEM were  
133 compiled to create a 30 m DEM of the completely covered study area.

134 **Table 1.** All DEMs collected in this study

DEM	Extent	Resolution	Access
NASADEM	[56°S, 61°N]	30 m	<a href="https://search.earthdata.nasa.gov/search">https://search.earthdata.nasa.gov/search</a>
ASTER GDEM v3	[83°S, 83°N]	30 m	<a href="https://gdemdl.aster.jspacesystems.or.jp/">https://gdemdl.aster.jspacesystems.or.jp/</a>
ArcticDEM	[55°N, 90°N]	2 m	<a href="https://earthengine.google.com/">https://earthengine.google.com/</a>
REMA	[60°S, 88°S]	2m / 8m	<a href="https://earthengine.google.com/">https://earthengine.google.com/</a>
Copernicus DEM	Global	30 m	<a href="https://panda.copernicus.eu/web/cds-catalogue/panda">https://panda.copernicus.eu/web/cds-catalogue/panda</a>

135 **Note:** The interval in the 'Extent' column represents all landmasses within a zonal range, but coverage may not exist  
136 for all areas.

137  
138 In addition, graphical data (Machguth and Huss, 2014) of glacier length in \*.xy format with an  
139 unknown projection coordinate system in High Asia were collected, which correspond to the  
140 attribute of the glacier maximum length ( $L_{max}$ ) in RGI v6.0. Because the data was obtained from an  
141 unofficial source, we could not access the data description documents and only recovered the  
142 coordinate matching between these points and some glaciers in RGI v6.0. Registration of the \*.xy  
143 file depends on the match between its filename and the feature identity document (FID) of the glacier  
144 polygon of RGI v6.0 in the same glacier area. The glacier lengths (MHMLDS) of successful  
145 registration were used as graphical validation data for this study.

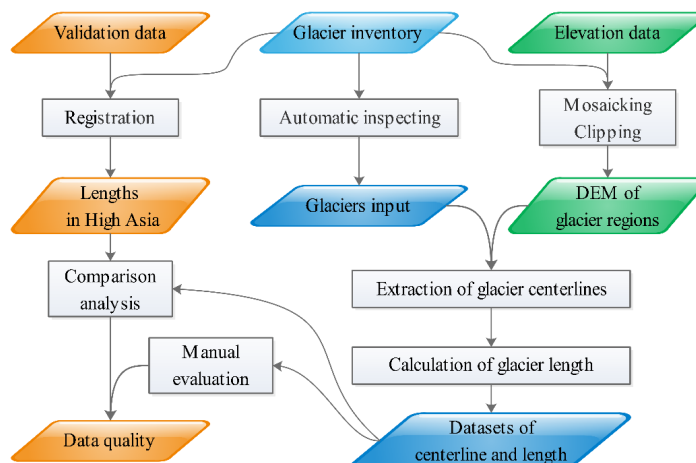
### 147 3 Methods

#### 148 3.1 Outline of workflow

149 This study relied on two key input datasets: global glacier inventory and compiled global glacier  
150 elevation. The goal of this study was to establish a new dataset of global graphic glacier centerlines  
151 and lengths. An outline of the workflow is shown in Figure 2. The process was divided into six parts:  
152 (1) design an algorithm to check all glacier outlines, marks, and exclude defective glacier polygons;  
153 (2) buffer glaciers to produce a mask containing global glaciers and their buffers; (3) mosaic



154 compiled global DEMs according to the masks in step 2 of different glacier regions to prepare the  
155 global glacier elevation data; (4) determine the automatic extraction parameters of glacier  
156 centerlines around the world by repeated testing in each region; (5) input the global DEM and glacier  
157 outline dataset and all parameters into the designed automatic extraction software (Zhang et al.,  
158 2021) to generate the centerlines and length in the global glacier; and (6) verify and compare with  
159 other centerline results obtained via different methods to evaluate the accuracy of the new datasets.



160

161

162

**Figure 2.** Workflow of the centerline and length dataset production.

163

### 3.2 Illustration of key methods

164

#### 3.2.1 Pre-process of glacier outlines

165

166

167

168

169

170

171

172

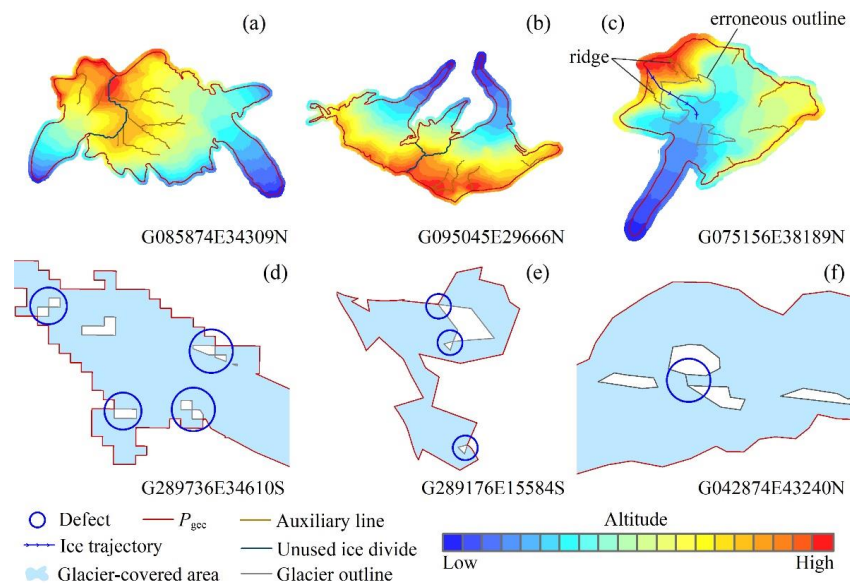
173

174

175

176

This study had strict requirements for glacier outlines, and all glacier complexes should be divided into individual glaciers before centerline extraction. However, because of the limited semi-automatic glacier segmentation approach (Kienholz et al., 2013) and the high-priority strategy of completeness of coverage adopted by RGI v6.0 (RGI Consortium, 2017), some glaciers were not supported by our algorithm. These glaciers included three categories: glacier complexes with/without inaccurate segmentation (Fig. 3a-b), incorrect glacier outlines (Fig. 3c), and flawed glaciers (Fig. 3d-f) generated by the automatic extraction algorithm. For the third category, we designed an identification algorithm (see paragraph 3) to mark and screen them. The flaws in these glacier outlines were mainly caused by topology errors of polylines/polygons, such as unclosed, sawtooth, and overlap. The first two categories do not affect the program's normal operation; however, the accuracy of the extraction results is difficult to guarantee. We cannot identify them at present and a solution is needed to improve the quality of the global glacier inventory.



177

178 **Figure 3.** Schematic of three types of flawed glacier outlines. **(a-b)** Glacier complexes with/without  
 179 inaccurate segmentation. **(c)** Incorrect glacier outline. **(d-f)** Panels represent three common  
 180 problems in flawed glaciers: defects in automatic algorithm, defects in post-processing, and artificial  
 181 errors. Auxiliary line represents lower-grade ice divide in the individual glacier, which is part of the  
 182 ridge lines.

183

184 In this study, we defined the external contour of a glacier ( $P_{gcc}$ ), namely, the polygon corresponding  
 185 to the longest closed polyline of the glacier, to reduce the storage of DEMs and improve the  
 186 efficiency of batch processing. The buffer masks of all glaciers (buffer distance: approximately 100  
 187 m) were generated by their  $P_{gcc}$  to meet the requirement for the extent of input DEMs to be slightly  
 188 larger than the  $P_{gcc}$ . The buffer masks generated initially were relatively broken because there are  
 189 overlaps or gaps between the adjacent polygons of the buffer zone. We merged small spots to remove  
 190 polygons with a perimeter less than 12 times the buffer distance on the glacier buffer masks of each  
 191 region.

192

193 The third category of glaciers (Fig. 3d-f) with flaws was identified by obtaining  $P_{gcc}$ . In the third  
 194 category, the most common type is two or more closed polylines with the same endpoint in a glacier.  
 195 There were also a few glacier polygons with false closed polylines, which are the head and tail  
 196 endpoints of the polylines that do not coincide, but the distance is less than the tolerance. The  
 197 solution was as follows: flawed glacier outlines were identified by judging whether there were  
 198 multiple polylines sharing endpoints after converting the glacier from a polygon to polylines, but  
 199 these outlines do not include the false closed type.

200

### 201 3.2.2 Preparation of input datasets

202 All data were processed in units of first-order glacier regions. The input glacier outlines excluded  
 203 all the defective glacier outlines. Similarly, the nominal glaciers (represented by an ellipse) and ice





204 caps remarked in RGI v6.0 were also treated, which were distinguished by two attributes: status  
 205 (nominal glacier) and form (ice cap). The inspection results (Table 2) of glacier outlines show that  
 206 there are 10,764 defective glacier outlines (*FGODS*) in RGI v6.0, accounting for approximately  
 207 4.97% of the total (216,502). After excluding nominal glaciers (461) and ice caps (7,174), 198,646  
 208 glaciers remained as input glacier outlines (*IGODS*), accounting for 91.75% of the total global  
 209 mountain glaciers.

210 **Table 2.** Preprocessing results of different glacier regions and information of input datasets.

Region	Region Name	Total	Ice Cap	Nominal glacier	Flawed glacier	Glacier input	DEM input
R01	Alaska	27108	0	0	704	26404	NASADEM, GDEM
R02	Western Canada and USA	18855	0	0	1564	17291	NASADEM, GDEM
R03	Arctic Canada, North	4556	650	0	47	3869	COP DEM
R04	Arctic Canada, South	7415	953	0	63	6409	NASADEM, GDEM
R05	Greenland Periphery	20261	1658	0	1547	17247	COP DEM
R06	Iceland	568	133	0	1	435	GDEM
R07	Svalbard	1615	144	0	12	1460	GDEM
R08	Scandinavia	3417	0	4	75	3338	NASADEM, GDEM
R09	Russian Arctic	1069	460	0	0	609	GDEM
R10	North Asia	5151	5	116	136	4899	COP DEM
R11	Central Europe	3927	0	2	76	3849	NASADEM
R12	Caucasus Middle East	1888	0	339	2	1547	NASADEM
R13	Central Asia	54429	1545	0	28	52858	NASADEM
R14	South Asia West	27988	295	0	1946	25792	NASADEM
R15	South Asia East	13119	289	0	4	12826	NASADEM
R16	Low Latitudes	2939	0	0	724	2215	NASADEM
R17	Southern Andes	15908	623	0	3828	11734	NASADEM
R18	New Zealand	3537	0	0	0	3537	NASADEM
R19	Antarctic Subantarctic	2752	419	0	7	2327	COP DEM
--	--	216502	7174	461	10764	198646	--

211 **Note:** GDEM and COP DEM represent ASTER GDEM v3 and Copernicus DEM, respectively.

212  
 213  $P_{\text{gec}}$  of all glaciers in RGI v6.0 constitute the global glacier external contour dataset (*GGECDs*),  
 214 which generated the buffer mask dataset (*GGBMDS*) of global mountain glaciers. The collected  
 215 DEMs were extracted using *GGBMDS* and 43,035 DEM tiles were generated. They were then  
 216 mosaicked according to different first-order glacier regions to generate a global glacier elevation  
 217 dataset (*GGEDs*). The details of the two input datasets are presented in Table 2.

218  
 219 **3.2.3 Generation of centerline and glacier length**

220 The automatic extraction tool of ‘GlacierCenterlines\_Py27’ (Update to version 5.2.1) was used,  
 221 which is based on the axis concept and Euclidean allocation (Zhang et al., 2021). The principle is  
 222 briefly explained as follows: the highest and lowest points of the external outline of a glacier as two  
 223 endpoints were extracted, cells with the equal shortest distances from the cell to both sides were  
 224 identified in a glacier polygon, and the line formed by these cells was regarded as the glacier  
 225 centerline. The maximum length of a glacier was calculated using an algorithm similar to the critical  
 226 path. The updated contents focused on formulating the parameterization scheme (Appendix A: Table  
 227 A1) for extracting global glacier centerlines, as well as repairing some newly discovered bugs, such  
 228 as a dead cycle in the process of auxiliary line extraction. All glacier outlines included in the *IGODS*  
 229 were divided into ten levels (Table 3) using the proportion of cumulative area after ranking the area  
 230 of all input glacier polygons from small to large. User-defined Albers with WGS1984 as the



231 reference ellipsoid were used as a unified projection coordinate system. The central meridian,  
 232 standard parallel 1, standard parallel 2, and origin latitude of the different glacier regions were  
 233 determined by their spatial extent. The empirical values of the other parameters were determined in  
 234 repeated attempts and their values had a significant correlation with glacier scale. The glacier  
 235 centerlines generated were merged according to the glacier regions and the graphics and attribute  
 236 information of glacier length were exported as corresponding independent ESRI shapefiles. In  
 237 addition, some key associated data were exported, such as the segmentation results of glacier  
 238 outlines, the lengths in the accumulation and ablation region of each glacier, the lowest points, the  
 239 local highest points ( $P_{max}$ ), the failed glacier outlines dealt, and logs.

**Table 3.** Statistics of global glaciers by different levels.

Level	Count	Area/km <sup>2</sup>	Acc. area/km <sup>2</sup>	Percent	Interval/km <sup>2</sup>
L1	165593	1.00	41313.79	10%	[0.01, 1.00]
L2	22833	3.57	82629.47	20%	(1.00, 3.57]
L3	6906	11.39	123947.69	30%	(3.57, 11.39]
L4	2149	35.51	165282.14	40%	(11.39, 35.51]
L5	698	103.10	206631.32	50%	(35.51, 103.10]
L6	262	248.26	247917.55	60%	(103.10, 248.26]
L7	113	521.40	289227.71	70%	(248.26, 521.40]
L8	55	1087.47	330595.34	80%	(521.40, 1087.47]
L9	27	2657.74	374312.14	90%	(1087.47, 2657.74]
L10	10	6004.85	413136.71	100%	(2657.74, 6004.85]
Total	198646	--	--	--	--

241

### 242 3.2.4 Accuracy assessment

243 A random assessment was prioritized in this study. We randomly selected 100 glaciers in each  
 244 glacier region and obtained 19 samples with a total of 1,900 glacier centerlines. These glacier  
 245 centerlines were divided by artificial inspection into three first-level categories (Zhang et al., 2021):  
 246 correct (I), inaccurate (II), and incorrect (III). Type II mostly contains glaciers with accurate glacier  
 247 maximum lengths but missing, redundant, or unreasonable branches of glacier centerlines. When  
 248 calculating verification accuracy, Types I and II were regarded as correct, and only Type III was  
 249 considered incorrect. Finally, the glacier proportion of Type III in the sample was counted and the  
 250 valuation result ( $R$ ) was calculated using Eq. (1).

$$251 \quad R = \sum_{i=1}^{19} \frac{S_i \times N_{T_i}}{N_G}, \quad (1)$$

252 where  $N_G$  is the total quantity of glaciers and  $N_{T_i}$  and  $S_i$  are the verification accuracy and number of  
 253 glaciers in the corresponding glacier region of the  $i$  th sample ( $i = 1, 2, 3, \dots, 18, 19$ ), respectively.

254 All glacier maximum lengths ( $G_{L,max}$ ) in this study were compared with the  $L_{max}$  (Machguth and  
 255 Huss, 2014) in RGI v6.0 using linear correlation and ratio analysis. Here, we took  $L_4 - L_{10}$  at the  
 256 glacier level as the same grade for statistics. The correlations between  $G_{L,max}$  and  $L_{max}$  were  
 257 established according to different glacier regions and glacier levels and the length ratio,  $R_r$  (Eq. 2),  
 258 was calculated. In addition, considering the differences between the graphics, we also collected  
 259 graph data of glacier length extracted by Machguth and Huss (2014). Considering the limited  
 260 availability of data (obtained: R13–R15), we only compared two glacier-covered regions in the  
 261 Himalayas: Mount Qomolangma and Kangchenjunga (the world's third-highest mountain) and their  
 262 surrounding areas.





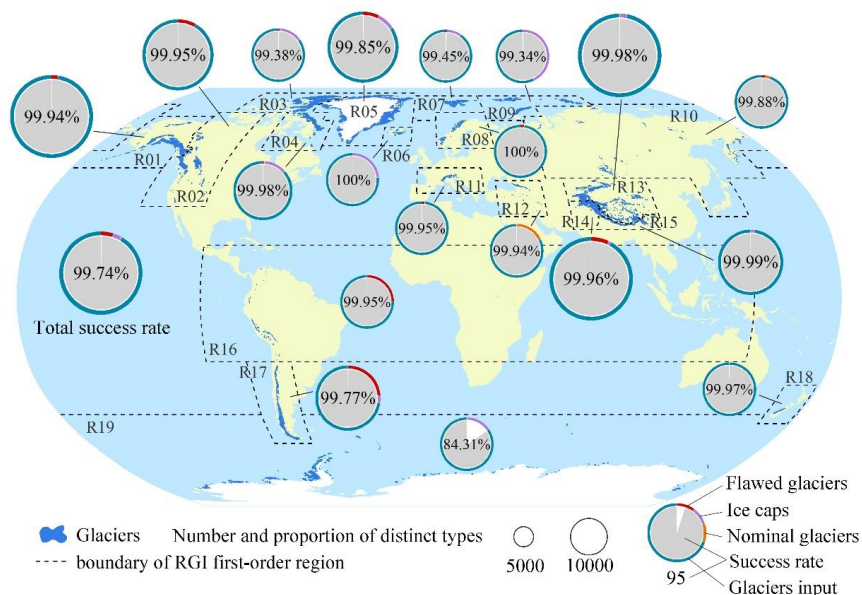
$$R_r = \frac{G_{L_{\max}}}{L_{\max}} \quad (2)$$

264

265 **4 Results**

266 **4.1 Centerline and length of glaciers**

267 Taking the *IGODS*, *GGEDS*, and other model parameters as input data, 198,137 glacier centerlines  
 268 were automatically generated using the centerline extraction tool of 'GlacierCenterlines\_Py27  
 269 v5.2.1', with a success rate of 99.74%. The number and proportion of flawed glacier outlines,  
 270 nominal glaciers, ice caps, input glacier outlines, and extraction results for distinct glacier regions  
 271 are shown in Fig. 4.



272

273 **Figure 4.** Extraction results of glacier centerlines in different glacier regions. The ring in the pie  
 274 chart represents the proportion of input glacier number and the number of excluded three glacier  
 275 types with total number of glaciers in the region. Pie chart represents the correct rate, which is the  
 276 proportion of the extraction result number with input glacier quantity. The size of the pie/ring  
 277 represents the grade of the glacier number in the region.

278

279 Except for Antarctica and Subantarctica (R19), the success rates of extracting glacier centerlines in  
 280 other glacier regions were greater than 99%, which indicates that the automatic extraction algorithm  
 281 for glacier centerlines is robust. A small number of glacier outlines with false closed problems and  
 282 unidentified ice caps were the main reasons for the failure of automatic extraction of glacier  
 283 centerlines; however, it is difficult to establish rules for accurately identifying these glacier polygons.  
 284 In total, 510 unsuccessful glacier outlines were identified, of which Antarctic-Subantarctic (R19)  
 285 accounted for 71.57%; Southern Andes (R17) and Greenland Periphery (R05) for 5.29% and 5.1%,  
 286 respectively; Arctic Canada North (R03) and Alaska (R01) for 4.71% and 2.94%, respectively; and  
 287 other glacier regions for less than 2%.



288

289 Overall, the global glacier centerline dataset (*GGCLDS*) constructed in this study contained 91.52%  
 290 of the total glaciers in RGI v6.0. The lengths of each branch of the glacier centerline were derived  
 291 and the longest branch lengths of the glacier centerline were defined as the glacier maximum length  
 292 ( $G_{Lmax}$ ), which were used to form the global glacier maximum length dataset (*GGMLDS*). The  
 293 average centerline length of all branches of a glacier is called the glacier mean length ( $G_{Lmean}$ ). In  
 294 addition, the median glacier altitude was regarded as the equilibrium line altitude (ELA) (Machguth  
 295 and Huss, 2014), the part with  $G_{Lmax}$  higher than ELA was regarded as the length of the glacier  
 296 accumulation zone ( $G_{Lacc}$ ), and the part lower than ELA was regarded as the length of the glacier  
 297 ablation zone ( $G_{Labl}$ ), which formed the glacier accumulation zonal length dataset (*GACLDS*) and  
 298 glacier ablation zone length dataset (*GABLDS*). The key process data corresponding to *GGCLDS*  
 299 were also output, to form the glacier outline segmentation results (*GOSRDS*), lowest points  
 300 (*GGLPDS*), local highest points (*GLHPDS*), and unsuccessful glacier outlines (*GUGODS*). The  
 301 fields involved in all datasets are explained in Table 4.

302

**Table 4.** Description of the attributes contained in all datasets.

Name	Data type	Char. length	Description
GLIMS_ID	Char.	14	Unique code of a glacier
Type	Long int.	4	Glacier grade in this study
MaxL	Float	8	Glacier maximum length (Unit: m)
MeanL	Float	8	Glacier average length (Unit: m)
ELA	Long int.	4	Equilibrium line altitude (Unit: m)
AccL	Float	8	Length in the accumulation region (Unit: m)
AblationL	Float	8	Length in the ablation region (Unit: m)
Id	Long int.	8	Data code of the same glacier
BS	Long int.	8	Tag of the same segment in a glacier
RASTERVALU	Long int.	4	Altitude of a $P_{max}$ (Unit: m)

303

**Note:** Char. and int. represent Character and integer, respectively.

304

305 The glacier outlines of RGI v6.0 without centerline results in this study were limited by the quality  
 306 of the glacier polygons, which mainly correspond to the flawed glacier outlines (*FGODS*), and the  
 307 identified ice caps in RGI v6.0. Among the *FGODS* (10,764), Southern Andes (R17) had the most,  
 308 followed by Southwest Asia (R14); Western Canada and USA (R02) and Greenland Periphery (R05),  
 309 with slightly more than 1,500; and Low Latitudes (R16) and Alaska (R01), with slightly more than  
 310 700. There were 451 in other glacier regions, including two regions with 0 defective glacier outline,  
 311 the Russian Arctic (R09) and New Zealand (R18). Among the ice caps (7174) identified by RGI  
 312 v6.0, slightly more than 1,500 were in R05 and Central Asia (R13), between 500 and 1,000 in the  
 313 Arctic Canada South (R04), Arctic Canada North (R03), and R17, and less than 500 in other glacier  
 314 regions. Nominal glaciers (461) existed in three glacial regions: Caucasus Middle East (R12), North  
 315 Asia (R10), and Scandinavia (R08).

316

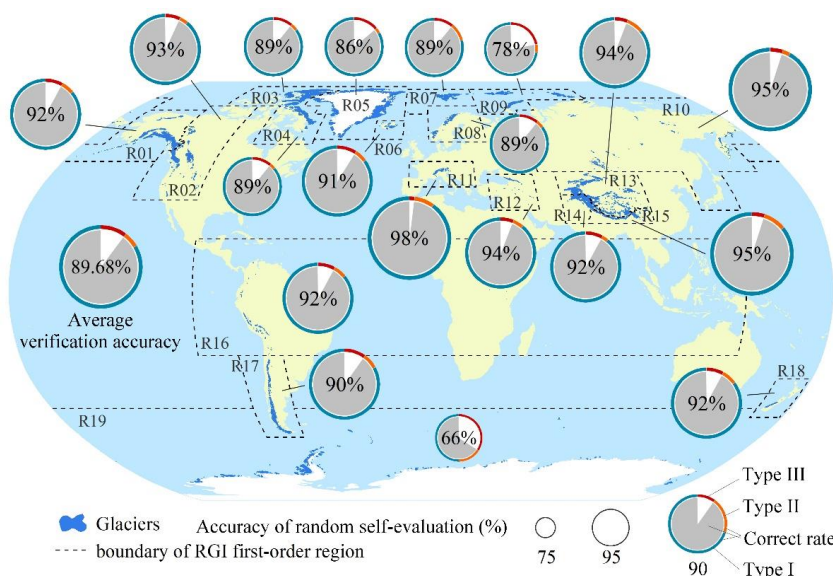
## 317 4.2 Data validation

### 318 4.2.1 Random self-assessment results

319 The evaluation results using random samples from the glacier centerline dataset suggested that the  
 320 average verification accuracy of the glacier centerline dataset was 89.68%. There were significant  
 321 differences in the accuracy of the 19 glacier regions around the world (Fig. 5). Among them, R11,  
 322 R15 and R10, R09, and R19 were the highest (98%), second highest (95%), slowest lower (78%),  
 323 and lowest (50%), respectively. In terms of types, the average proportions of Types I and II were



324 83.53% and 6.16%, respectively. The proportion of Type I in R07 and R09 was relatively low, at  
 325 79% and 73%, respectively, and the lowest in R19 was only 50%. Type II had the highest proportion  
 326 in R19 at 16%, followed by R07 (10%). Moreover, Type II accounted for more than 5% in seven  
 327 regions: R11, R13, R17, R18, R16, R01, and R06.



328

329 **Figure 5.** Statistical chart of random evaluation results. The ring in the pie chart represents the  
 330 proportion of each type with total number of samples in the region. Pie chart represents the correct  
 331 rate, which is the proportion of the number of Types I and II with region sample quantity. The size  
 332 of the pie/ring represents the grade of the correct rate in the region. Types I, II, and III (See Section  
 333 3.2.4) represent the centerline of correct, inaccurate, and incorrect, respectively.

334

335 The above results indicate that, in addition to the three glacier regions of R07, R09, and R19, the  
 336 random samples of the glacier centerline dataset have excellent performance in terms of accuracy,  
 337 particularly in R02, R12, and R14. The unmarked ice cap and local low-quality DEM were the main  
 338 reasons for the poor quality of the glacier centerline in R07 and R09, respectively. Owing to glacier  
 339 complexes and low altitude differences in low-quality DEMs at the glacier tongue, the quality of  
 340 the glacier centerline obtained in R19 was poor. However, from the viewpoint of dataset coverage,  
 341 we provided the extraction results of the glacier centerline in R19.

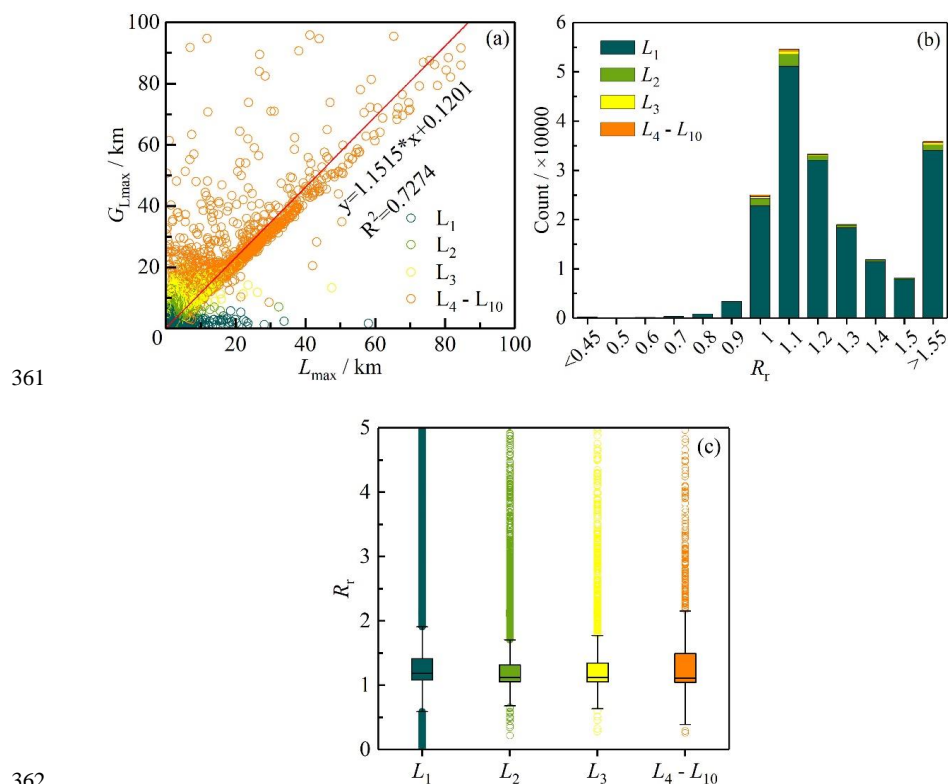
342

#### 343 4.2.2 Compare with previous results

344 After applying this algorithm to the global glacier inventory RGI v6.0, we compared the glacier  
 345 lengths ( $G_{L_{max}}$ ) automatically obtained in this study with those ( $L_{max}$ ) obtained by Machguth and  
 346 Huss (2014) (Fig. 6). After eliminating 5408 glaciers with  $L_{max}$  value of -9 (no results), the length  
 347 values of the other 192728 glaciers in the global glacier length dataset were directly compared. The  
 348  $G_{L_{max}}$  and  $L_{max}$  were generally comparable (Fig. 6a). The glaciers in grades  $L_4$ – $L_{10}$  showed excellent  
 349 fitting degrees, while those of  $L_1$ – $L_3$  determined the linear correlation coefficient owing to their  
 350 large number. The number of glaciers with a length ratio ( $R_l$ ) between  $G_{L_{max}}$  and  $L_{max}$  greater than



351 1.55 (Fig. 6b) was approximately 35,000, which were excluded from histogram statistics because  
 352 there was a high probability that the length of at least one of the two datasets was erroneous. The  
 353 peak value of the histogram (Fig. 6b) of  $R_r$  is in the interval 1.05–1.15 and  $R_r$  in the interval 0.95–  
 354 1.25 accounts for 64.55%. The glacier length  $G_{L_{\max}}$  in this study was generally longer than  $L_{\max}$  and  
 355 the average value was approximately 10%, which indicates that glacier centerline lengths were  
 356 probably underestimated in previous studies. In addition, the abnormal value of the length ratio of  
 357 glacier  $L_1$  was the highest and the median value was high (Fig. 6c). The  $R_r$  values of glaciers  $L_4$ – $L_{10}$   
 358 fluctuated greatly. The  $R_r$  distributions of glaciers  $L_2$  and  $L_3$  were relatively concentrated. The reason  
 359 for this is that the length of glacier  $L_1$  was affected by the DEM, while glaciers  $L_4$ – $L_{10}$  were mainly  
 360 disturbed by differences in glacier scale and the accuracy of the auxiliary line.



362  
 363 **Figure 6.** Comparison of longest centerlines calculated in this study and by Machguth and Huss  
 364 (2014). **(a)** Linear regression of maximum length for all input glaciers ( $IGODS$ ), determined in the  
 365  $G_{L_{\max}}$ , calculated in this study and  $L_{\max}$  obtained in Machguth and Huss (2014). **(b)** Histogram of  
 366 length ratio ( $R_r$ ,  $G_{L_{\max}}/L_{\max}$ ) for distinct grades of glaciers. **(c)** Box plots of length ratio ( $R_r$ ) for  
 367 different scales of glaciers.

368  
 369 Comparisons between  $G_{L_{\max}}$  and  $L_{\max}$  for each first-order glacier region and all random samples are  
 370 shown in Appendix B. There was a preferable fitting degree between  $G_{L_{\max}}$  and  $L_{\max}$  in seven glacier  
 371 regions including R01, R04, R07, and R12–R15, in which the  $R^2$  was larger than 0.95 (Fig. B1).  
 372 The  $R_r$  in R17 ( $R^2 = 0.8174$ ), R05 ( $R^2 = 0.8136$ ), and R03 ( $R^2 = 0.6311$ ) were poor, whereas that in



373 R19 ( $R^2 = 0.5487$ ) was the worst. The  $R^2$  values of the other eight glacier regions were between 0.85  
374 and 0.95. The histograms (Fig. B2) suggest that  $\hat{G}_{L_{\max}}$  and  $L_{\max}$  fitted well in R04, R06, R07, R09,  
375 and R12–R15 because they had recognizable single peak values. The peak values of R03, R05, R17,  
376 and R19 were not prominent and the proportion of glaciers with  $R_r > 1.55$  was extremely high,  
377 further increasing the uncertainty in glacier length results in these four regions. R01, R07, R08,  
378 R11–R15, and R18 performed well in the box plot (Fig. B3), whereas the results for R09 were not  
379 good. Moreover, the fitting degree of all random samples was poor (Fig. B1,  $R^2 = 0.7547$ ), the peak  
380 value was more prominent (Fig. B2), and the length ratio distribution of glaciers of different grades  
381 was relatively scattered (Fig. B3). In general, the glacier lengths of R07 and R12–R15 were the  
382 closest, while there were significant differences in R03, R05, R17, and R19.

383

384 Furthermore, graphic results collected for the maximum length of glaciers in parts of High Asia  
385 (Machguth and Huss, 2014) were used to compare the results. In two parts of R15, Mount  
386 Qomolangma and its surrounding area (Fig. 7a) and Kangchenjunga and its surrounding area (Fig.  
387 7b), the glaciers showed a flaky distribution for mapping. Visible comparison was suggested that  
388 the extraction method used in this study had likely a strong ability to obtain the maximum length of  
389 glaciers (Fig. 7a) and that its sensitivity to topography was lower than that of Machguth and Huss  
390 (2014) (Fig. 7b). Both sets of glacier length extraction schemes were valid and there were large  
391 differences only in a few glaciers or in certain types of glaciers, such as slope glaciers and ice caps.

392

393 Note that the comparative analysis results of the two lengths were relative, random samples were  
394 limited, and it was difficult to accurately reflect the quality of the dataset in this study. Owing to  
395 these limitations, the quality of the data must be determined again by secondary evaluation before  
396 applying to specific regions. Additionally, the automatic extraction algorithm in this study is more  
397 suitable for application to single-outlet glaciers, particularly valley glaciers; it is not suitable for ice  
398 caps, flat-top glaciers, and tidal glaciers that are widely distributed in the Antarctic, sub-Antarctic,  
399 northern Canadian Arctic, and other areas. Even if our algorithm can produce promising results,  
400 accuracy remains a concern.

401



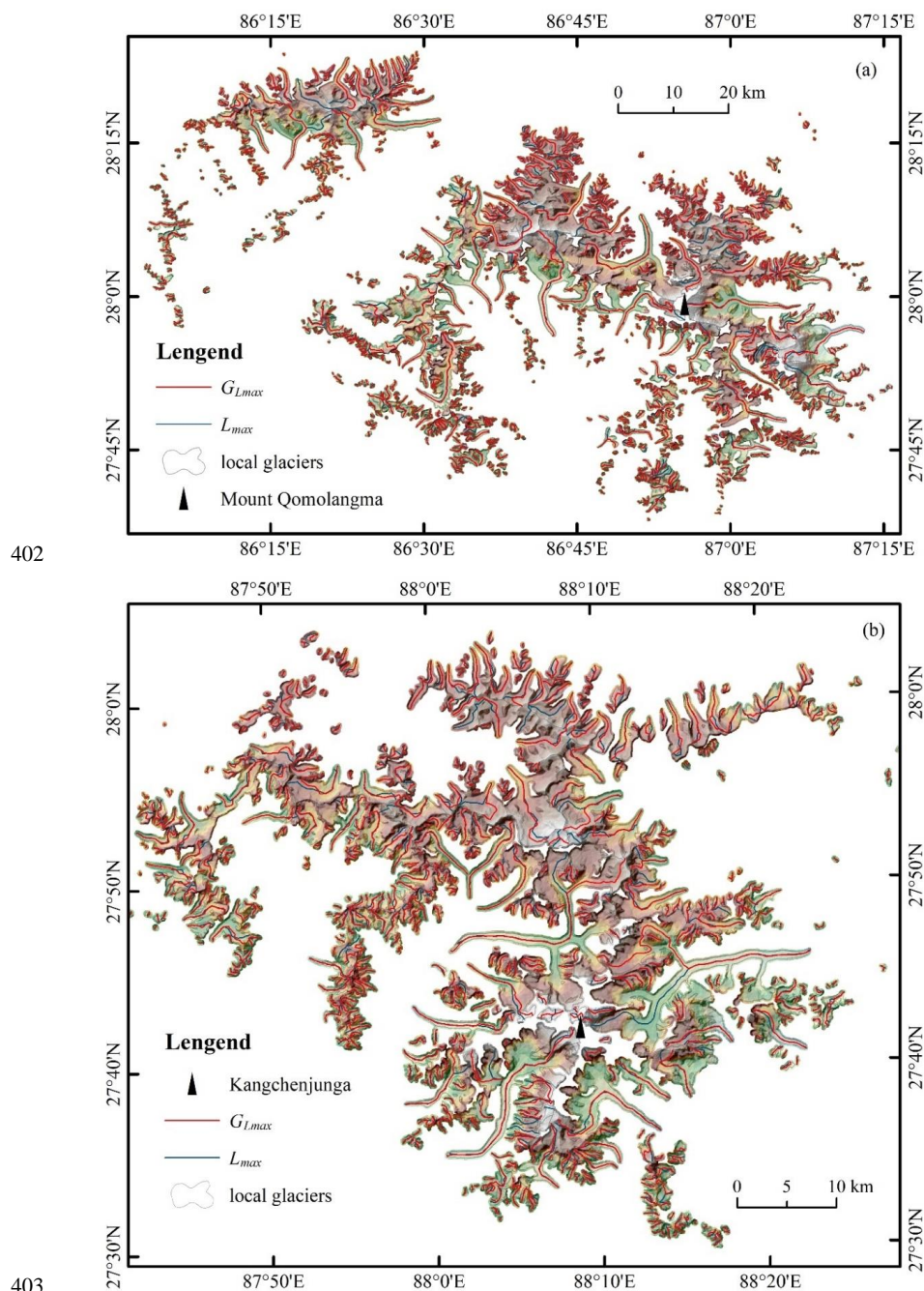


**Figure 7.** Visible comparison of the longest center lines calculated in this study and by Machguth and Huss (2014). The figure shows two glacier-covered regions in the Himalayas, covering Mount Qomolangma (**panel a**) and Kangchenjunga (**panel b**, the world's third highest mountain) and their surrounding areas. The background is the DEM used for the calculation.





## 408 5 Data availability

409 Global glacier centerline dataset (*GGCLDS*), global glacier maximum length dataset (*GGMLDS*),  
410 and other relevant datasets are available at <https://doi.org/10.11922/sciencedb.01643> (or  
411 <https://www.scidb.cn/en/s/BRzaUf>). All 14 sub-datasets of this dataset are listed in Table 5.

412 **Table 5.** Description of the members contained in this dataset.

Acronym	Data format	Data volume	Description
<i>IGODS</i>	*.shp	316 MB	Input glacier outline dataset
<i>GGEDS</i>	*.tif	3.70 GB	Global glacier elevation dataset
<i>GGCLDS</i>		838 MB	Global glacier centerline dataset
<i>GGMLDS</i>		616 MB	Global glacier maximum length dataset
<i>GACLDS</i>		302 MB	Global glacier accumulation region length dataset
<i>GABLDS</i>		358 MB	Global glacier ablation region length dataset
<i>GOSRDS</i>		1.16 GB	Global glacier outline segmentation result dataset
<i>GLHPDS</i>		11 MB	Global glacial local highest point dataset
<i>GLPDS</i>	*.shp	6.25 MB	Global glacial lowest point dataset
<i>GUGODS</i>		3.95 MB	Unsuccessful global glacier outline dataset
<i>FGODS</i>		119 MB	Global flawed glacier outline dataset
<i>GGECDs</i>		334 MB	Global glacier external contour dataset
<i>GGBMDS</i>		374 MB	Global glacier buffer mask dataset
<i>MHMLDS</i>		8.32 MB	The maximum length of Machguth and Huss in High Asia

413

## 414 6 Conclusions

415 In this study, a new dataset on the centerline of global glaciers was constructed and the maximum  
416 length was calculated based on the global glacier inventory (RGI v6.0) and global glacier region  
417 DEM (*GGEDS*, composed of NASADEM, ASTER GDEM v3, and Copernicus DEM). In total,  
418 198,137 glacier centerlines were generated, accounting for 99.74% of the total number of imported  
419 glaciers (*IGODS*) and 91.52% of the total number of the global glacier inventory. The  
420 comprehensive extraction accuracy of these glacier centerlines (*GGCLDS*) used in random self-  
421 assessment was 89.68%. The glacier length ( $G_{Lmax}$ ) obtained in this study was generally  
422 approximately 10% longer than that of  $L_{max}$  on average. Nevertheless, our method showed a stronger  
423 ability to obtain the maximum length, and we believe that the resulting errors were controllable.  
424 Furthermore, the preprocessing algorithm we designed accurately identified 10,764 erroneous  
425 glacier polygons from RGI v6.0, which formed the defective glacier dataset (*FGODS*).

426

427 A dataset containing 14 sub-datasets was generated through the above work, including two basic  
428 input datasets (*IGODS* and *GGEDS*), two key result datasets (*GGCLDS* and *GGMLDS*), four  
429 process datasets and six derived result datasets. Ice caps, nominal glaciers, and erroneous glacier  
430 polygons were eliminated from most sub-datasets in this study, accounting for approximately 8.25%  
431 of the total RGI v6.0. The poor status of these glacier polygons was not sufficient to support the  
432 automatic extraction of glacier centerlines, which needs to be improved in future work. Inevitably,  
433 there were some defects in the algorithm or datasets that need to be considered in future research.  
434 For instance, the glacial regions (R19 and R03) with the worst results were added to the dataset to  
435 prioritize data coverage integrity. It is worth noting that the global glacier DEM dataset (*GGEDS*),  
436 global glacier external outline dataset (*GGECDs*), and global glacier buffer mask datasets  
437 (*GGBMDS*) cover all glaciers in RGI v6.0. Accordingly, they will help researchers design more  
438 efficient automated extraction algorithms to produce datasets containing all types of glacier  
439 centerlines and lengths worldwide, which is our next goal.



440

441 **Appendix A:** Model parameters resulting from the Central Asia Glacier and extended to worldwide  
 442 calculations are listed in Table A1.

443 **Table A1.** Parameterization scheme for extracting global glacier centerlines.

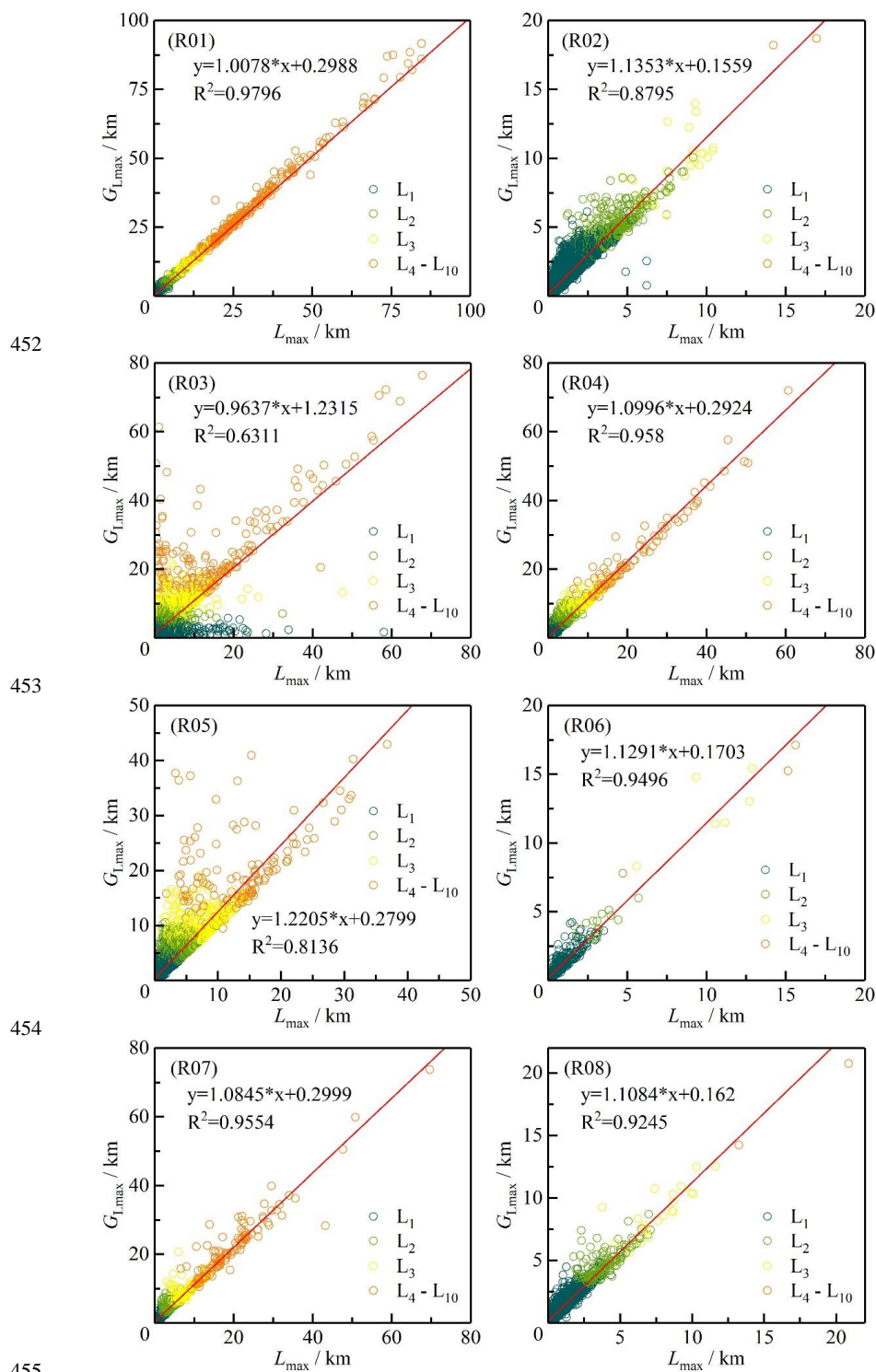
Par.	Description	Value (Levels 1-10)	Unit
$P_1$	Maximum distance between adjacent vertexes	10	m
$P_2$	Buffer distance outside the glacier outline	30	m
$P_3$	Threshold of accumulative flow	5 - 8, 10, 20, 30, 50, 100, 200	int $\times 10^3$
$P_4$	Length of the shortest auxiliary line	10 - 19	int
$P_5$	Length of the longest auxiliary line	2 - 11	int
$P_6$	Interval for searching the local highest points	50, 60, 70, 80, 90, 100, 200, 300, 400, 500	count
$P_7$	Matching tolerance of the vertexes of polyline	0.2, 0.2, 0.5, 0.5, 1 ( $L_5 - L_{10}$ )	m
$P_8$	Size of grid cell in Euclidean allocation	1, 5, 15, 15, 30 ( $L_5 - L_{10}$ )	m
$P_9$	Minimum distance between the adjacent $P_{\max}$	10, 15, 30, 60, 120, 150, 200, 300, 400, 500	count
$P_{10}$	Smoothing tolerance of polylines	5, 10, 15, 20, 30 ( $L_5 - L_{10}$ )	m
$P_{11}$	Length threshold of the longest auxiliary line	10190	km <sup>2</sup>

444 **Notes:** The calculation method for each parameter is detailed in Zhang et al. (2021).  $P_{\max}$  and  $L$  refer to the local  
 445 highest points and grades of the glacier, respectively.

446

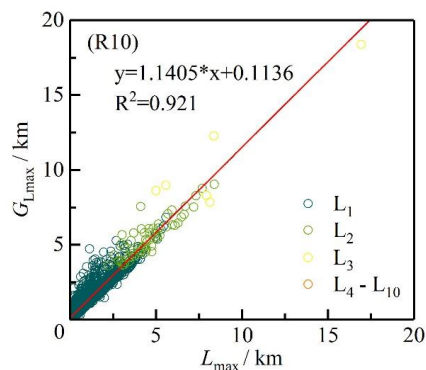
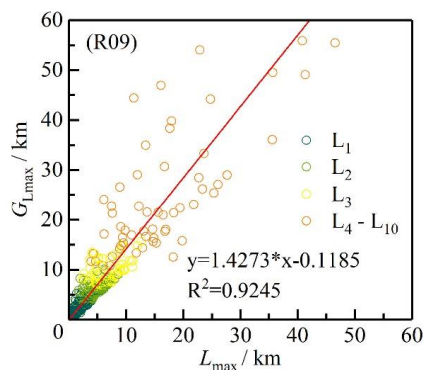
447 **Appendix B:** Comparison of longest centerlines calculated in this study and by Machguth and Huss  
 448 (2014) for all samples and the different first-order glacier regions of RGI v6.0. Linear regression of  
 449 the two lengths, histogram of length ratio ( $R_r$ ), and box plots of  $R_r$  for glaciers of different grades in  
 450 these regions were in Figure B1, B2, and B3, respectively.

451

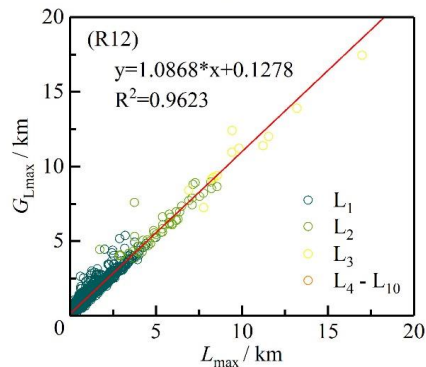
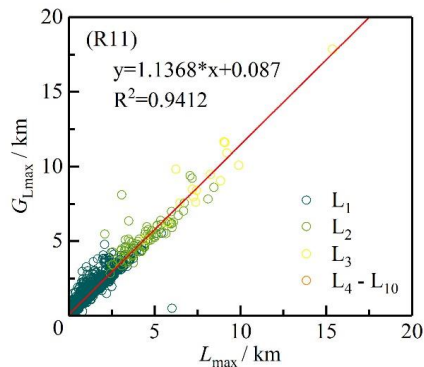




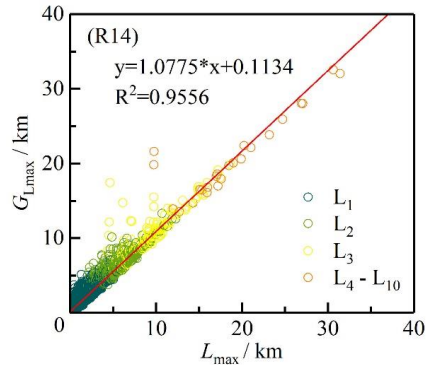
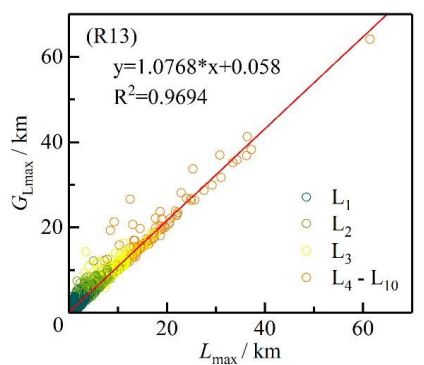
456



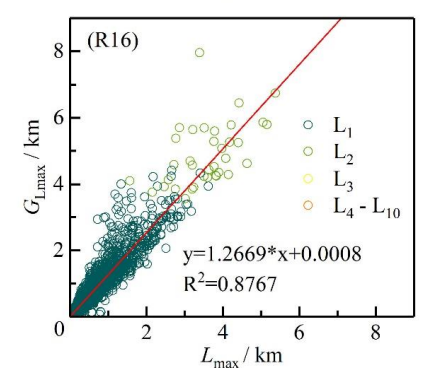
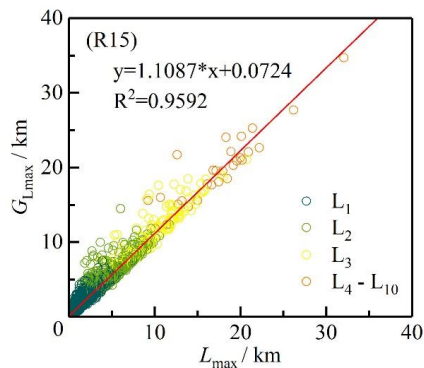
457

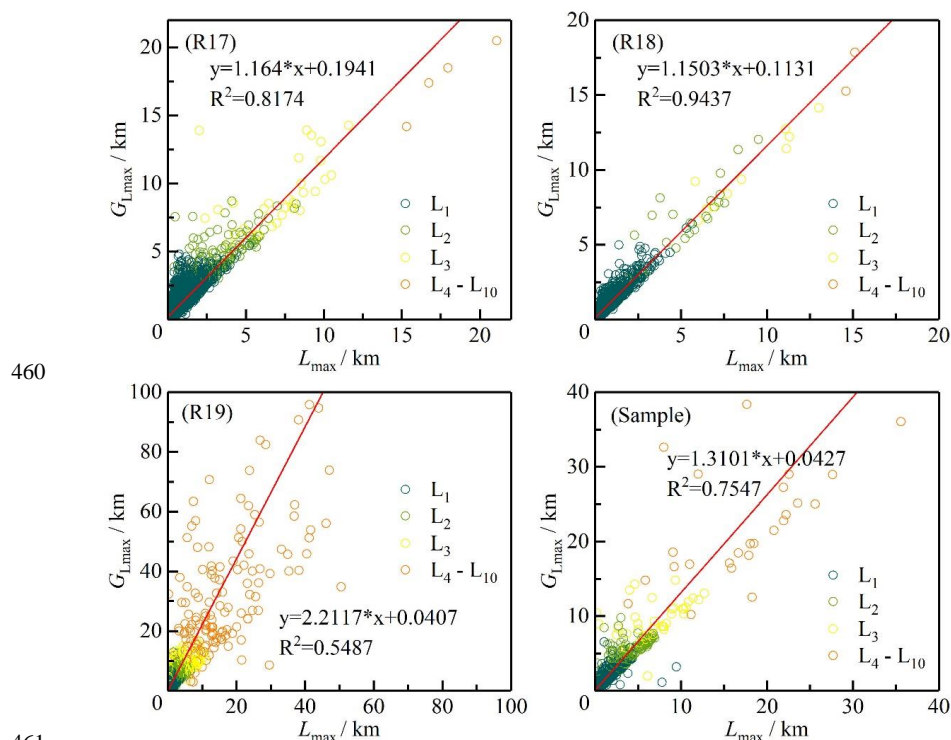


458

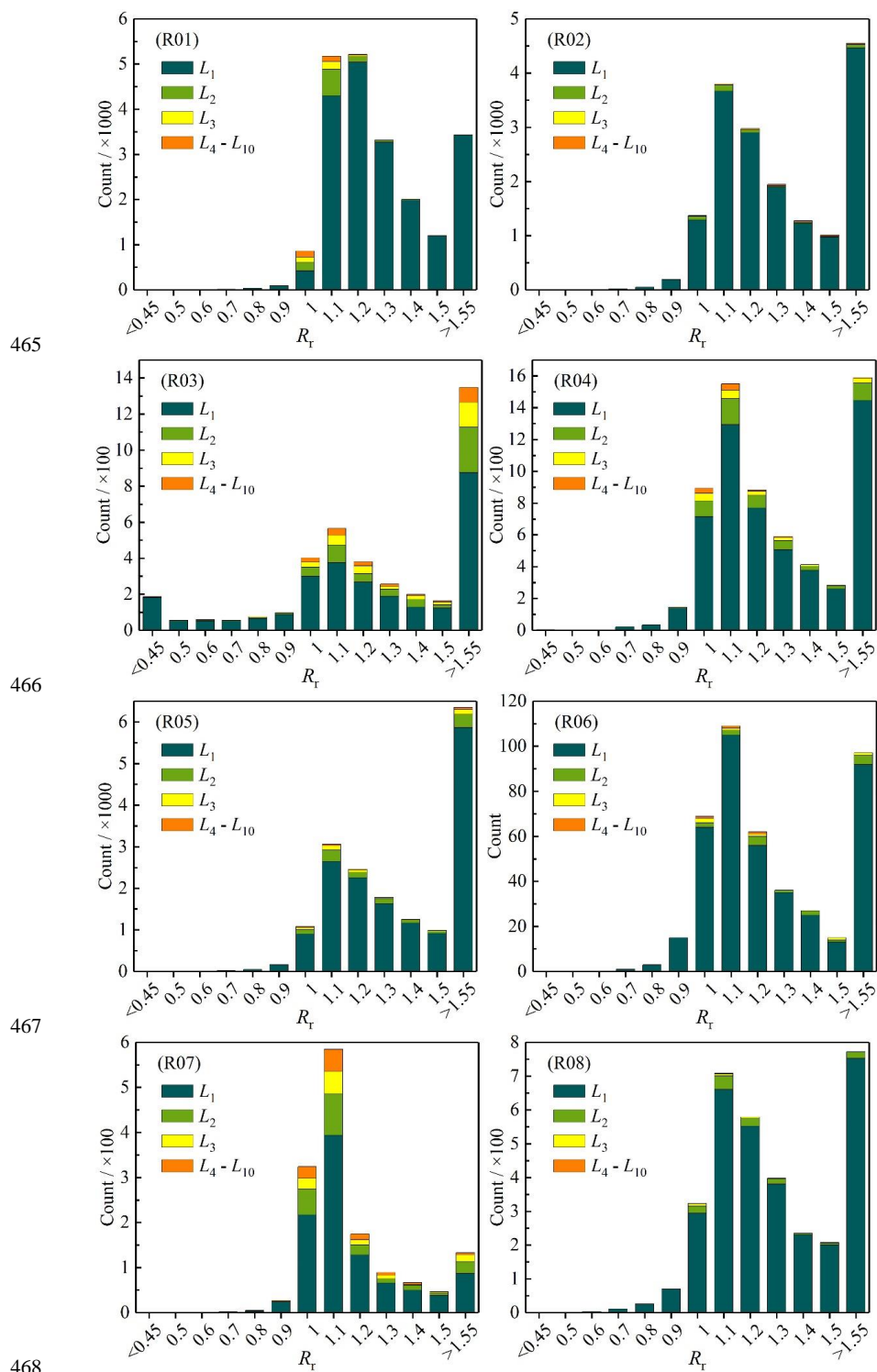


459





461  
462 **Figure B1.** Linear regression in different glacier regions between glacier length ( $G_{L_{max}}$ ) calculated  
463 in this study and glacier length ( $L_{max}$ ) calculated by Machguth and Huss (2014).  
464



465

466

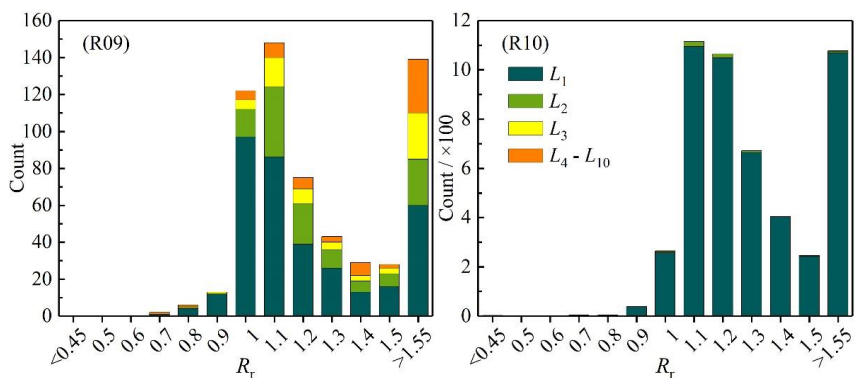
467

468

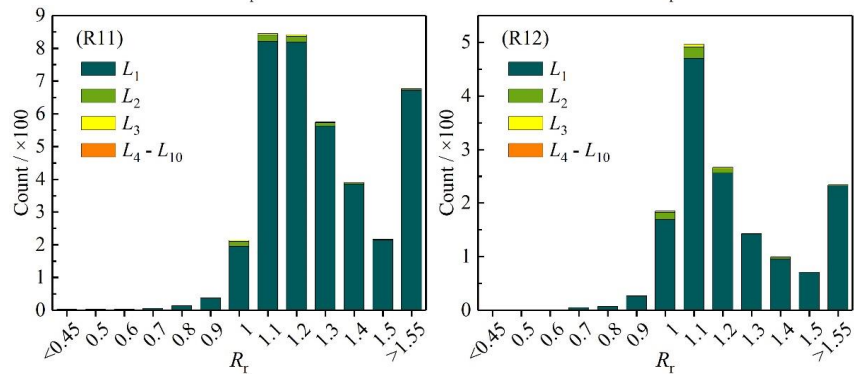




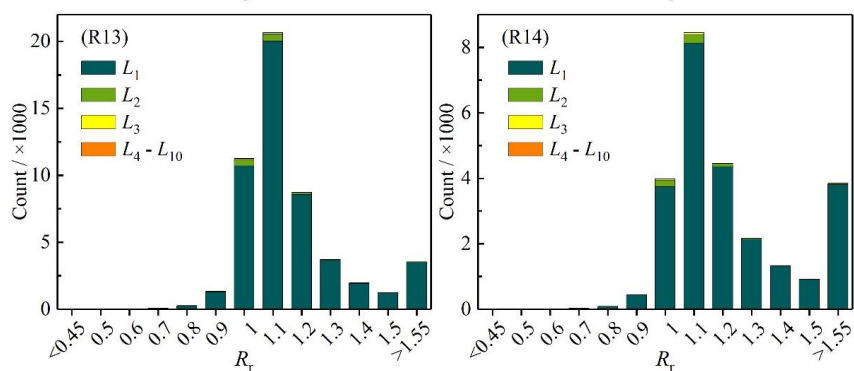
469



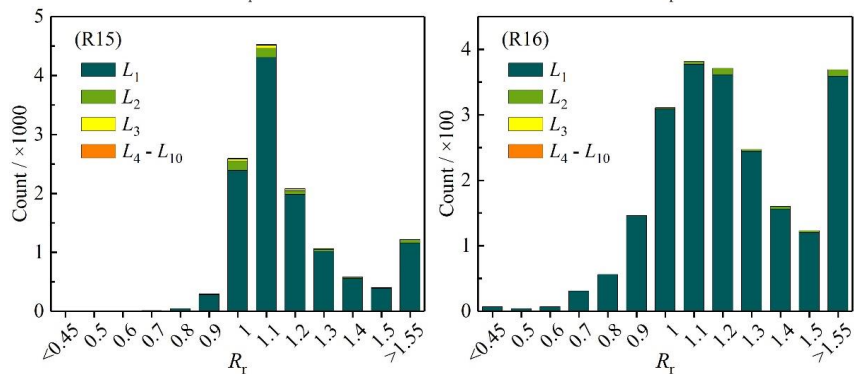
470

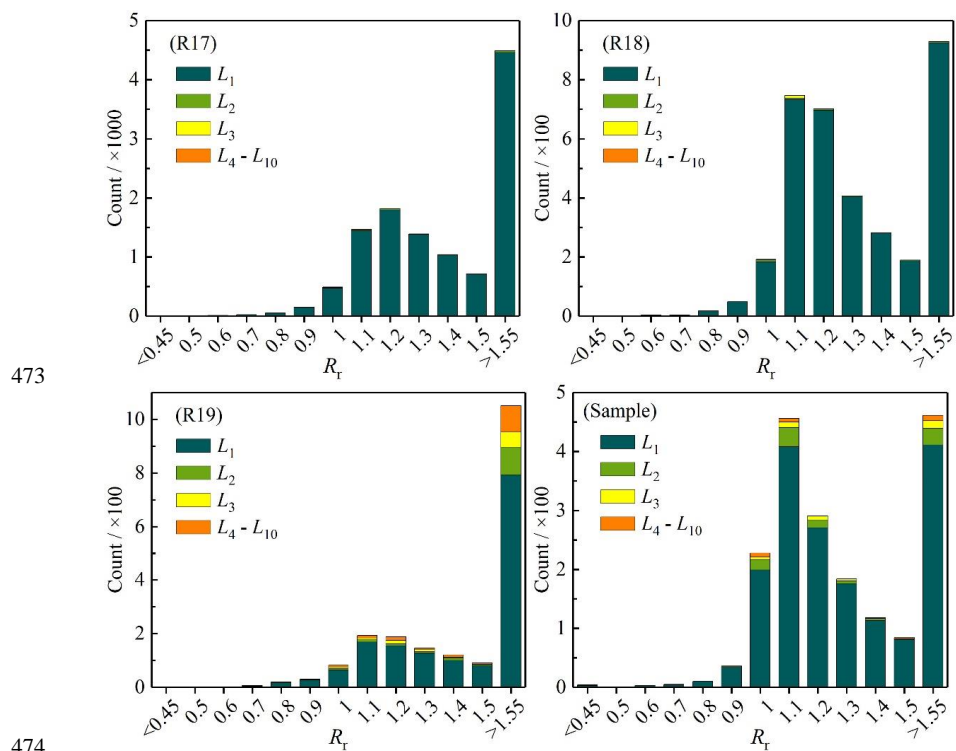


471



472





473

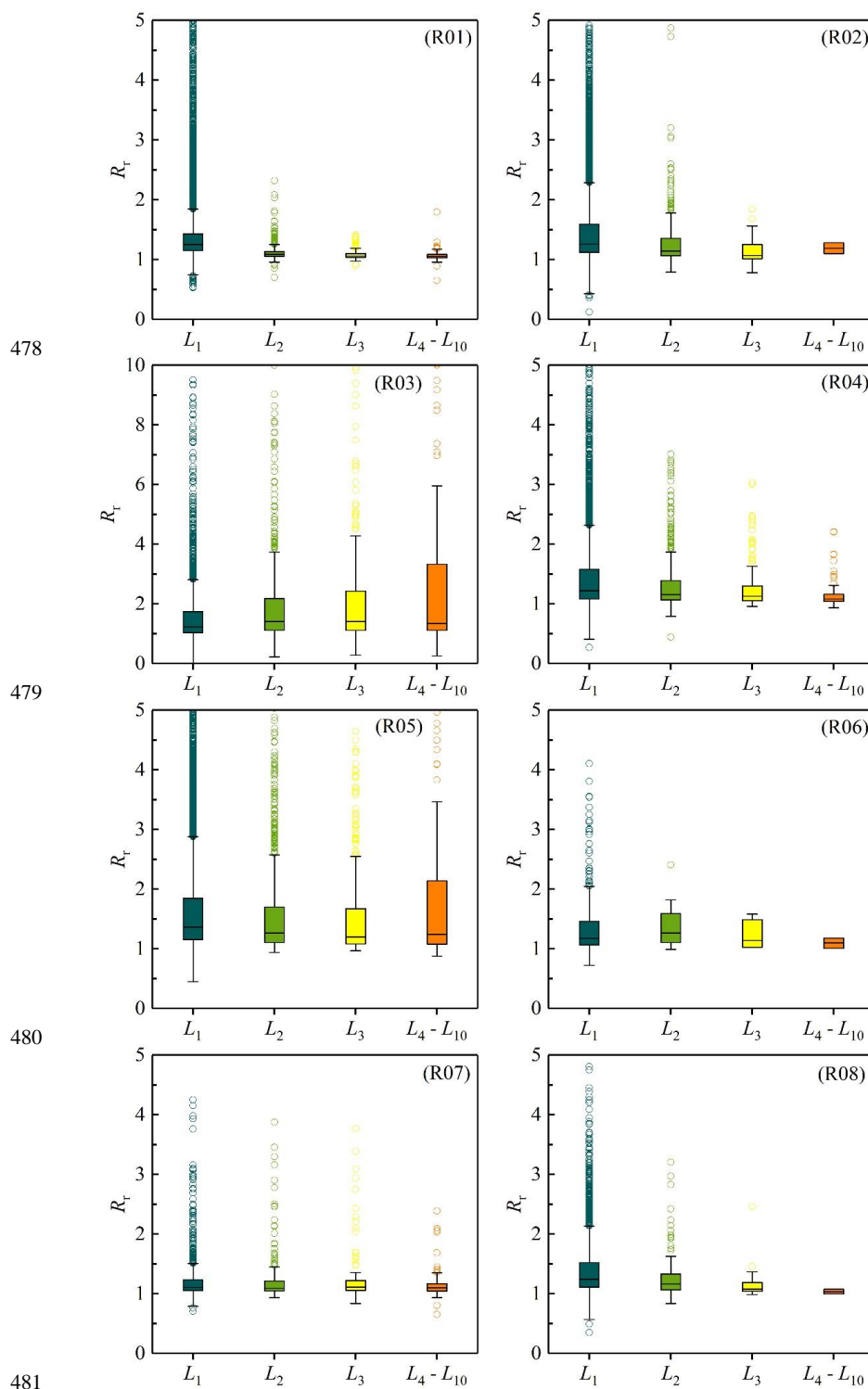
474

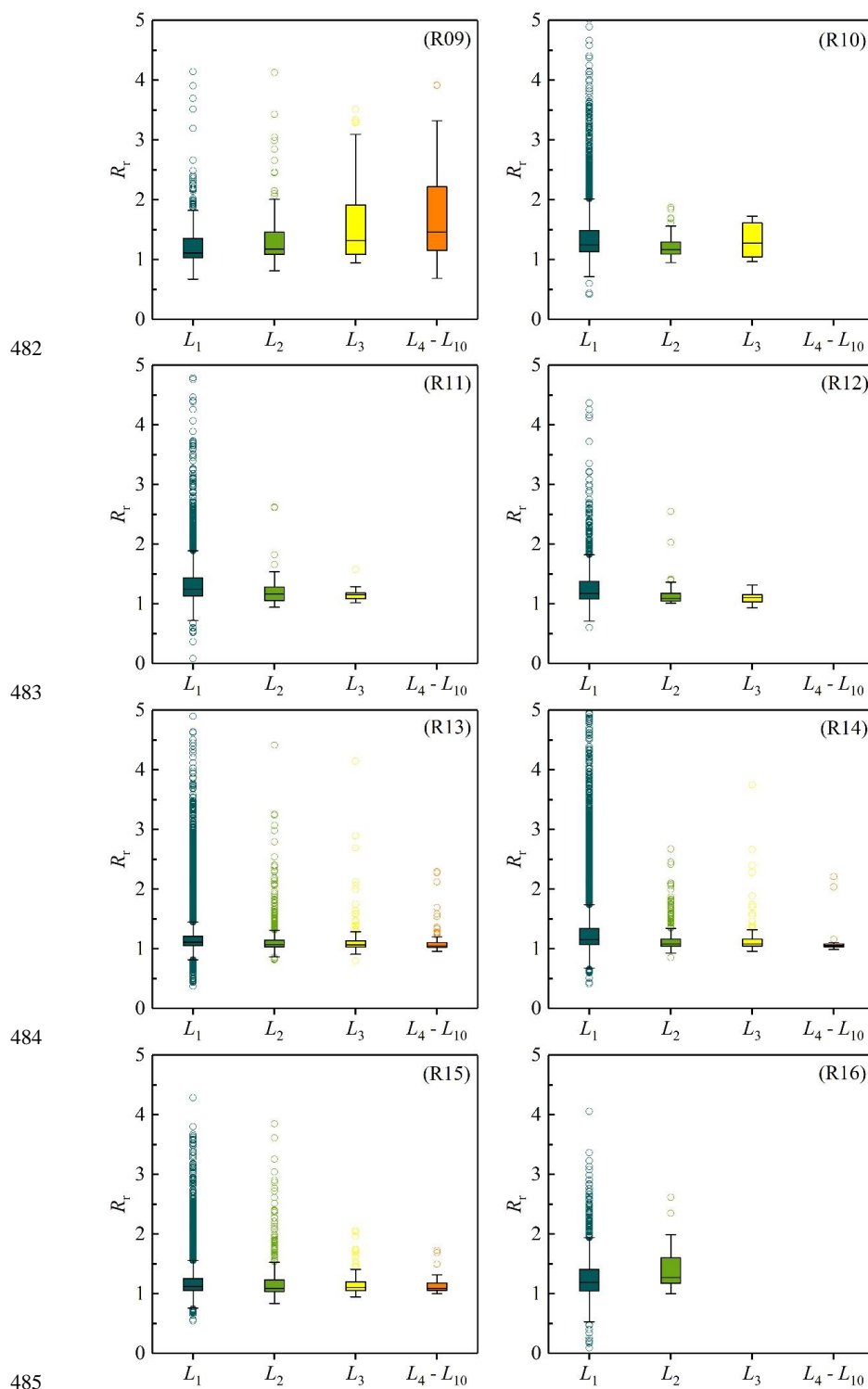
475

476

477

**Figure B2.** Histograms of the length ratio ( $R_r$ ,  $G_{L_{\max}}/L_{\max}$ ) of distinct glacier grades in glacier-covered regions and all samples.





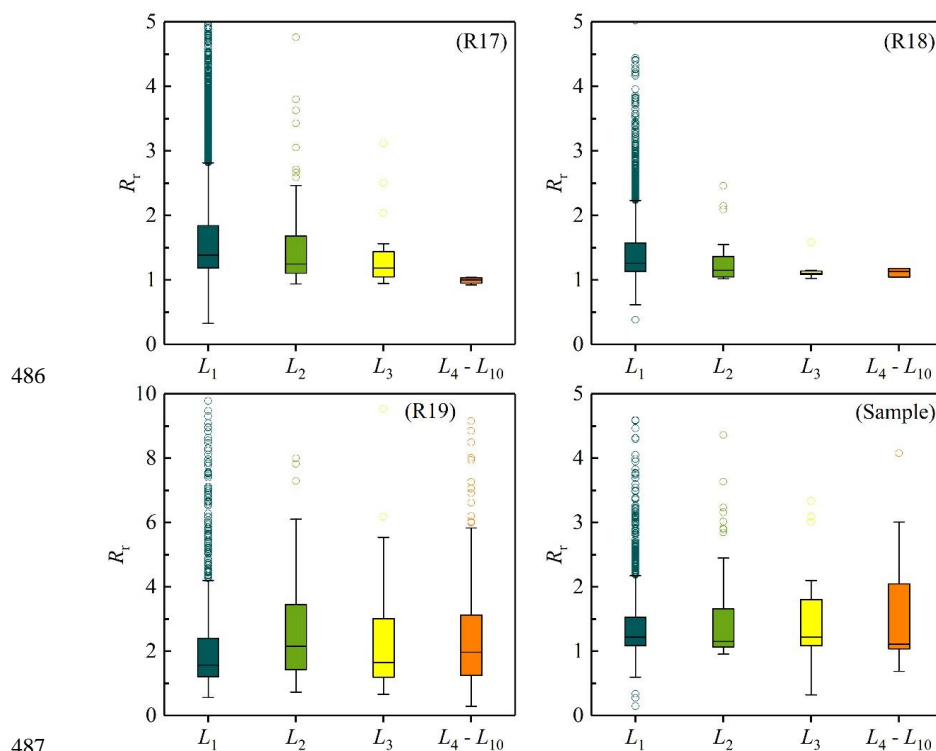


**Figure B3.** Box plots of length ratio ( $R_r$ ,  $G_{L_{max}}/L_{max}$ ) of glaciers of distinct grades in every glacier-covered region and whole sample.



491 **Supplement.**

492 The Supplement consists of two parts: (1) ‘GlacierCenterlines\_Py27’ (version 5.2.1), the updated  
493 automatic extraction tool of glacier centerlines in this study, which fixed some defects compared  
494 with version 5.2.0 (<https://doi.org/10.5194/tc-151955-2021-supplement>). (2)  
495 ‘Other\_parameters\_T1.txt’ is the parameter file for extracting the global glacier centerlines.

496

497 **Author contributions.**

498 All authors contributed to writing and editing the manuscript. DZ processed the data, performed all  
499 calculations, created all figures, and wrote most of the manuscript. SZ contributed significantly to  
500 the development of the analyses, figures, and writing. XY contributed to the development of the  
501 data production strategy and writing. GZ and WL contributed to the initial data production. SW  
502 participated in writing Chapter 4.

503

504 **Competing interests.**

505 The authors declare that they have no conflict of interest.

506

507 **Acknowledgments.**

508 The authors would especially like to thank GLIMS for releasing the RGI v6.0  
509 (<http://www.glims.org/RGI/andolph.html>, last accessed: November 15, 2021), LP DAAC for  
510 releasing the NASADEM (<https://lpdaac.usgs.gov/news/release-nasadem-data-products/>, last  
511 accessed: November 17, 2021), METI and NASA for jointly releasing the ASTER GDEM v3  
512 (<https://lpdaac.usgs.gov/news/nasa-and-meti-release-aster-global-dem-version-3/>, last accessed:  
513 November 17, 2021), and the European Space Agency (ESA) for providing the Copernicus DEM  
514 (<https://spacedata.copernicus.eu/web/cscda/cop-dem-faq>, last accessed: November 17, 2021). This  
515 work is not possible without the support of open-access data.

516

517 **Financial support.**

518 This research was funded by the Second Tibetan Plateau Scientific Expedition and Research  
519 Program (STEP) (grant number: 2019QZKK020109) and China National Natural Science  
520 Foundation (grant numbers: 41730751, 42171124).

521

522 **References**

- 523 Abrams, M., Crippen, R., and Fujisada, H.: ASTER Global Digital Elevation Model (GDEM) and  
524 ASTER Global Water Body Dataset (ASTWBD), Remote Sensing, 12,  
525 <https://doi.org/10.3390/rs12071156>, 2020.
- 526 Aciego, S. M., Stevenson, E. I., and Arendt, C. A.: Climate versus geological controls on glacial  
527 meltwater micronutrient production in southern Greenland, Earth and Planetary Science Letters,  
528 424, 51-58, <https://doi.org/10.1016/j.epsl.2015.05.017>, 2015.
- 529 Carabajal, C. C. and Boy, J. P.: Evaluation of Aster Gdem V3 Using Icesat Laser Altimetry, ISPRS -  
530 International Archives of the Photogrammetry, Remote Sensing and Spatial Information Sciences,  
531 XLI-B4, 117-124, <https://doi.org/10.5194/isprsarchives-XLI-B4-117-2016>, 2016.
- 532 Carrera-Hernández, J. J.: Not all DEMs are equal: An evaluation of six globally available 30 m resolution  
533 DEMs with geodetic benchmarks and LiDAR in Mexico, Remote Sensing of Environment, 261,  
534 <https://doi.org/10.1016/j.rse.2021.112474>, 2021.





- 535 Cazenave, A.: Global sea-level budget 1993–present, *Earth System Science Data*, 10, 1551-1590,  
536 <https://doi.org/10.5194/essd-10-1551-2018>, 2018.
- 537 Farinotti, D., Huss, M., Fürst, J. J., Landmann, J., Machguth, H., Maussion, F., and Pandit, A.: A  
538 consensus estimate for the ice thickness distribution of all glaciers on Earth, *Nature Geoscience*, 12,  
539 168-173, <https://doi.org/10.1038/s41561-019-0300-3>, 2019.
- 540 Farr, T. G., Rosen, P. A., Caro, E., Crippen, R., Duren, R., Hensley, S., Kobrick, M., Paller, M., Rodriguez,  
541 E., Roth, L., Seal, D., Shaffer, S., Shimada, J., Umland, J., Werner, M., Oskin, M., Burbank, D., and  
542 Alsdorf, D.: The Shuttle Radar Topography Mission, *Reviews of Geophysics*, 45, 1-33,  
543 <https://doi.org/10.1029/2005rg000183>, 2007.
- 544 Gao, Y. P., Yao, X. J., Liu, S. Y., Qi, M. M., Gong, P., An, L. N., Li, X. F., and Duan, H. Y.: Methods and  
545 future trend of ice volume calculation of glacier, *Arid Land Geography*, 41, 1204-1213,  
546 <https://doi.org/10.12118/j.issn.1000-6060.2018.06.08>, 2018.
- 547 Hansen, K., Hasenstab, K., and Schwartzman, A.: Estimating Mountain Glacier Flowlines by Local  
548 Linear Regression Gradient Descent, *IEEE Transactions on Geoscience and Remote Sensing*, 59,  
549 10022-10034, <https://doi.org/10.1109/tgrs.2020.3035513>, 2020.
- 550 Heid, T. and Kääh, A.: Repeat optical satellite images reveal widespread and long term decrease in land-  
551 terminating glacier speeds, *The Cryosphere*, 6, 467-478, <https://doi.org/10.5194/tc-6-467-2012>,  
552 2012.
- 553 Herla, F., Roe, G. H., and Marzeion, B.: Ensemble statistics of a geometric glacier length model, *Annals  
554 of Glaciology*, 58, 130-135, <https://doi.org/10.1017/aog.2017.15>, 2017.
- 555 Herreid, S. and Pellicciotti, F.: The state of rock debris covering Earth's glaciers, *Nature Geoscience*, 13,  
556 621-627, <https://doi.org/10.1038/s41561-020-0615-0>, 2020.
- 557 Howat, I. M., Porter, C., Smith, B. E., Noh, M.-J., and Morin, P.: The Reference Elevation Model of  
558 Antarctica, *The Cryosphere*, 13, 665-674, <https://doi.org/10.5194/tc-13-665-2019>, 2019.
- 559 Hugonnet, R., McNabb, R., Berthier, E., Menounos, B., Nuth, C., Girod, L., Farinotti, D., Huss, M.,  
560 Dussallant, I., Brun, F., and Kaab, A.: Accelerated global glacier mass loss in the early twenty-first  
561 century, *Nature*, 592, 726-731, <https://doi.org/10.1038/s41586-021-03436-z>, 2021.
- 562 Immerzeel, W. W., Lutz, A. F., Andrade, M., Bahl, A., Biemans, H., Bolch, T., Hyde, S., Brumby, S.,  
563 Davies, B. J., Elmore, A. C., Emmer, A., Feng, M., Fernández, A., Haritashya, U., Kargel, J. S.,  
564 Koppes, M., Kraaijenbrink, P. D. A., Kulkarni, A. V., Mayewski, P. A., Nepal, S., Pacheco, P., Painter,  
565 T. H., Pellicciotti, F., Rajaram, H., Rupper, S., Sinisalo, A., Shrestha, A. B., Viviroli, D., Wada, Y.,  
566 Xiao, C., Yao, T., and Baillie, J. E. M.: Importance and vulnerability of the world's water towers,  
567 *Nature*, 577, 364-369, <https://doi.org/10.1038/s41586-019-1822-y>, 2019.
- 568 Ji, Q., Yang, T.-b., He, Y., Qin, Y., Dong, J., and Hu, F.-s.: A simple method to extract glacier length based  
569 on Digital Elevation Model and glacier boundaries for simple basin type glacier, *Journal of  
570 Mountain Science*, 14, 1776-1790, <https://doi.org/10.1007/s11629-016-4243-5>, 2017.
- 571 Kääh, A., Jacquemart, M., Gilbert, A., Leinss, S., Girod, L., Huggel, C., Falaschi, D., Ugalde, F., Petrakov,  
572 D., Chernomorets, S., Dokukin, M., Paul, F., Gascoin, S., Berthier, E., and Kargel, J. S.: Sudden  
573 large-volume detachments of low-angle mountain glaciers – more frequent than thought?, *The  
574 Cryosphere*, 15, 1751-1785, <https://doi.org/10.5194/tc-15-1751-2021>, 2021.
- 575 Kienholz, C., Hock, R., and Arendt, A. A.: A new semi-automatic approach for dividing glacier  
576 complexes into individual glaciers, *Journal of Glaciology*, 59, 925-937,  
577 <https://doi.org/10.3189/2013JoG12J138>, 2013.
- 578 Kienholz, C., Rich, J. L., Arendt, A. A., and Hock, R.: A new method for deriving glacier centerlines



- 579 applied to glaciers in Alaska and northwest Canada, *The Cryosphere*, 8, 503-519,  
580 <https://doi.org/10.5194/tc-8-503-2014>, 2014.
- 581 Le Bris, R. and Paul, F.: An automatic method to create flow lines for determination of glacier length: A  
582 pilot study with Alaskan glaciers, *Computers & Geosciences*, 52, 234-245,  
583 <https://doi.org/10.1016/j.cageo.2012.10.014>, 2013.
- 584 Le Moine, N. and Gsell, P.-S.: A graph-based approach to glacier flowline extraction: An application to  
585 glaciers in Switzerland, *Computers & Geosciences*, 85, 91-101,  
586 <https://doi.org/10.1016/j.cageo.2015.09.010>, 2015.
- 587 Leclercq, P. W. and Oerlemans, J.: Global and hemispheric temperature reconstruction from glacier  
588 length fluctuations, *Climate Dynamics*, 38, 1065-1079, <https://doi.org/10.1007/s00382-011-1145-7>,  
589 2011.
- 590 Leclercq, P. W., Oerlemans, J., Basagic, H. J., Bushueva, I., Cook, A. J., and Le Bris, R.: A data set of  
591 worldwide glacier length fluctuations, *The Cryosphere*, 8, 659-672, [https://doi.org/10.5194/tc-8-  
592 659-2014](https://doi.org/10.5194/tc-8-659-2014), 2014.
- 593 Li, H., Ng, F., Li, Z., Qin, D., and Cheng, G.: An extended “perfect-plasticity” method for estimating ice  
594 thickness along the flow line of mountain glaciers, *Journal of Geophysical Research: Earth Surface*,  
595 117, n/a-n/a, <https://doi.org/10.1029/2011jf002104>, 2012.
- 596 Li, X., Ding, Y., Hood, E., Raiswell, R., Han, T., He, X., Kang, S., Wu, Q., Yu, Z., Mika, S., Liu, S., and  
597 Li, Q.: Dissolved Iron Supply from Asian Glaciers: Local Controls and a Regional Perspective,  
598 *Global Biogeochemical Cycles*, 33, 1223-1237, <https://doi.org/10.1029/2018gb006113>, 2019.
- 599 Li, Y., Li, F., Shangguan, D., and Ding, Y.: A new global gridded glacier dataset based on the Randolph  
600 Glacier Inventory version 6.0, *Journal of Glaciology*, 67, 773-776,  
601 <https://doi.org/10.1017/jog.2021.28>, 2021.
- 602 Lüthi, M. P., Bauder, A., and Funk, M.: Volume change reconstruction of Swiss glaciers from length  
603 change data, *Journal of Geophysical Research*, 115, <https://doi.org/10.1029/2010jf001695>, 2010.
- 604 Machguth, H. and Huss, M.: The length of the world's glaciers – a new approach for the global calculation  
605 of center lines, *The Cryosphere*, 8, 1741-1755, <https://doi.org/10.5194/tc-8-1741-2014>, 2014.
- 606 Maussion, F., Butenko, A., Champollion, N., Dusch, M., Eis, J., Fourteau, K., Gregor, P., Jarosch, A. H.,  
607 Landmann, J., Oesterle, F., Recinos, B., Rothenpieler, T., Vlug, A., Wild, C. T., and Marzeion, B.:  
608 The Open Global Glacier Model (OGGM) v1.1, *Geoscientific Model Development*, 12, 909-931,  
609 <https://doi.org/10.5194/gmd-12-909-2019>, 2019.
- 610 Melkonian, A. K., Willis, M. J., and Pritchard, M. E.: Satellite-derived volume loss rates and glacier  
611 speeds for the Juneau Icefield, Alaska, *Journal of Glaciology*, 60, 743-760,  
612 <https://doi.org/10.3189/2014JoG13J181>, 2017.
- 613 Noel, B., Jakobs, C. L., van Pelt, W. J. J., Lhermitte, S., Wouters, B., Kohler, J., Hagen, J. O., Luks, B.,  
614 Reijmer, C. H., van de Berg, W. J., and van den Broeke, M. R.: Low elevation of Svalbard glaciers  
615 drives high mass loss variability, *Nat Commun*, 11, 4597, [https://doi.org/10.1038/s41467-020-  
616 18356-1](https://doi.org/10.1038/s41467-020-18356-1), 2020.
- 617 Oerlemans, J.: A flowline model for Nigardsbreen, Norway: projection of future glacier length based on  
618 dynamic calibration with the historic record, *Annals of Glaciology*, 24, 382-389,  
619 <https://doi.org/10.1017/S0260305500012489> 1997.
- 620 Pfeffer, W. T., Arendt, A. A., Bliss, A., Bolch, T., Cogley, J. G., Gardner, A. S., Hagen, J.-O., Hock, R.,  
621 Kaser, G., Kienholz, C., Miles, E. S., Moholdt, G., Mølg, N., Paul, F., Radić, V., Rastner, P., Raup,  
622 B. H., Rich, J., and Sharp, M. J.: The Randolph Glacier Inventory: a globally complete inventory of



- 623 glaciers, *Journal of Glaciology*, 60, 537-552, <https://doi.org/10.3189/2014JoG13J176>, 2014.
- 624 Pritchard, H. D.: Asia's shrinking glaciers protect large populations from drought stress, *Nature*, 569,  
625 649-654, <https://doi.org/10.1038/s41586-019-1240-1>, 2019.
- 626 Radić, V. and Hock, R.: Regional and global volumes of glaciers derived from statistical upscaling of  
627 glacier inventory data, *Journal of Geophysical Research*, 115, <https://doi.org/10.1029/2009jf001373>,  
628 2010.
- 629 RGI Consortium: Randolph Glacier Inventory – A Dataset of Global Glacier Outlines: Version 6.0:  
630 Technical Report, Global Land Ice Measurements from Space, Colorado, USA, 10.7265/N5-RGI-  
631 60, 2017.
- 632 Scherler, D., Wulf, H., and Gorelick, N.: Global Assessment of Supraglacial Debris-Cover Extents,  
633 *Geophysical Research Letters*, 45, 11,798-711,805, <https://doi.org/10.1029/2018gl080158>, 2018.
- 634 Schiefer, E., Menounos, B., and Wheate, R.: An inventory and morphometric analysis of British  
635 Columbia glaciers, Canada, *Journal of Glaciology*, volume 54, 551-560, 2008.
- 636 Shukla, A., Garg, S., Mehta, M., Kumar, V., and Shukla, U. K.: Temporal inventory of glaciers in the  
637 Suru sub-basin, western Himalaya: impacts of regional climate variability, *Earth System Science*  
638 *Data*, 12, 1245-1265, <https://doi.org/10.5194/essd-12-1245-2020>, 2020.
- 639 Shukla, T. and Sen, I. S.: Preparing for floods on the Third Pole, *Science*, 372, 232-234,  
640 <https://doi.org/10.1126/science.abh3558>, 2021.
- 641 Sommer, C., Malz, P., Seehaus, T. C., Lippl, S., Zemp, M., and Braun, M. H.: Rapid glacier retreat and  
642 downwasting throughout the European Alps in the early 21(st) century, *Nat Commun*, 11, 3209,  
643 <https://doi.org/10.1038/s41467-020-16818-0>, 2020.
- 644 Stuart-Smith, R. F., Roe, G. H., Li, S., and Allen, M. R.: Increased outburst flood hazard from Lake  
645 Palcacocha due to human-induced glacier retreat, *Nature Geoscience*, 14, 85-90,  
646 <https://doi.org/10.1038/s41561-021-00686-4>, 2021.
- 647 Sugiyama, S., Bauder, A., Zahno, C., and Funk, M.: Evolution of Rhonegletscher, Switzerland, over the  
648 past 125 years and in the future : application of an improved flowline model, *Annals of Glaciology*,  
649 46, 268-274, 2007.
- 650 Thogersen, K., Gilbert, A., Schuler, T. V., and Malthe-Sorensen, A.: Rate-and-state friction explains  
651 glacier surge propagation, *Nat Commun*, 10, 2823, <https://doi.org/10.1038/s41467-019-10506-4>,  
652 2019.
- 653 Uuemaa, E., Ahi, S., Montibeller, B., Muru, M., and Kmoch, A.: Vertical Accuracy of Freely Available  
654 Global Digital Elevation Models (ASTER, AW3D30, MERIT, TanDEM-X, SRTM, and  
655 NASADEM), *Remote Sensing*, 12, <https://doi.org/10.3390/rs12213482>, 2020.
- 656 Vargo, L. J., Anderson, B. M., Dadić, R., Horgan, H. J., Mackintosh, A. N., King, A. D., and Lorrey, A.  
657 M.: Anthropogenic warming forces extreme annual glacier mass loss, *Nature Climate Change*, 10,  
658 856-861, <https://doi.org/10.1038/s41558-020-0849-2>, 2020.
- 659 Winsvold, S. H., Andreassen, L. M., and Kienholz, C.: Glacier area and length changes in Norway from  
660 repeat inventories, *The Cryosphere*, 8, 1885-1903, <https://doi.org/10.5194/tc-8-1885-2014>, 2014.
- 661 Wu, K., Liu, S., Jiang, Z., Liu, Q., Zhu, Y., Yi, Y., Xie, F., Ahmad Tahir, A., and Saifullah, M.:  
662 Quantification of glacier mass budgets in the Karakoram region of Upper Indus Basin during the  
663 early twenty-first century, *Journal of Hydrology*, 603,  
664 <https://doi.org/10.1016/j.jhydrol.2021.127095>, 2021.
- 665 Xia, W.: An Automatic Extraction Method of Glacier Length Based on Voronoi Algorithm - A Pilot Study  
666 in the Sanjiangyuan Region, College of Urban and Environmental Science, Northwest University,



- 667 Xi'an, Shannxi, 2020.
- 668 Yang, B. Y., Zhang, L. X., Gao, Y., Xiang, Y., Mou, N. X., and Suo, L. D. B.: An integrated method of  
669 glacier length extraction based on Gaofen satellite data, *Journal of Glaciology and Geocryology*, 38,  
670 1615-1623, <https://doi.org/10.7522/j.issn.1000-0240.2016.0189>, 2016.
- 671 Yao, X. J., Liu, S. Y., Zhu, Y., Gong, P., An, L. N., and Li, X. F.: Design and implementation of an  
672 automatic method for deriving glacier centerlines based on GIS, *Journal of Glaciology and*  
673 *Geocryology*, 37, 1563-1570, <https://doi.org/10.7522/j.issn.1000-0240.2015.0173>, 2015.
- 674 Zemp, M., Huss, M., Thibert, E., Eckert, N., McNabb, R., Huber, J., Barandun, M., Machguth, H.,  
675 Nussbaumer, S. U., Gartner-Roer, I., Thomson, L., Paul, F., Maussion, F., Kutuzov, S., and Cogley,  
676 J. G.: Global glacier mass changes and their contributions to sea-level rise from 1961 to 2016,  
677 *Nature*, 568, 382-386, <https://doi.org/10.1038/s41586-019-1071-0>, 2019.
- 678 Zhang, D. and Zhang, S.: A new global dataset of mountain glacier centerline and length, *Science Data*  
679 *Bank*, <https://doi.org/10.11922/sciencedb.01643>, 2022.
- 680 Zhang, D., Yao, X., Duan, H., Liu, S., Guo, W., Sun, M., and Li, D.: A new automatic approach for  
681 extracting glacier centerlines based on Euclidean allocation, *The Cryosphere*, 15, 1955-1973,  
682 <https://doi.org/10.5194/tc-15-1955-2021>, 2021.
- 683 Zheng, G., Allen, S. K., Bao, A., Ballesteros-Cánovas, J. A., Huss, M., Zhang, G., Li, J., Yuan, Y., Jiang,  
684 L., Yu, T., Chen, W., and Stoffel, M.: Increasing risk of glacial lake outburst floods from future Third  
685 Pole deglaciation, *Nature Climate Change*, 11, 411-417, [https://doi.org/10.1038/s41558-021-01028-](https://doi.org/10.1038/s41558-021-01028-3)  
686 [3](https://doi.org/10.1038/s41558-021-01028-3), 2021.
- 687 Zhou, S., Yao, X., Zhang, D., Zhang, Y., Liu, S., and Min, Y.: Remote Sensing Monitoring of Advancing  
688 and Surging Glaciers in the Tien Shan, 1990–2019, *Remote Sensing*, 13,  
689 <https://doi.org/10.3390/rs13101973>, 2021a.
- 690 Zhou, Y., Li, X., Zheng, D., Li, Z., An, B., Wang, Y., Jiang, D., Su, J., and Cao, B.: The joint driving  
691 effects of climate and weather changes caused the Chamoli glacier-rock avalanche in the high  
692 altitudes of the India Himalaya, *Science China Earth Sciences*, 64, 1909-1921,  
693 <https://doi.org/10.1007/s11430-021-9844-0>, 2021b.
- 694